NAVAL POSTGRADUATE SCHOOL
Monterey, California

THESIS

SAND BED ROUGHNESS IN THE NEARSHORE, COAST 3D EXPERIMENT, EGMOND AAN ZEE, THE NETHERLANDS

by

Robert L. Kendall

June 2000

Thesis Advisor: Edith L. Gallagher
Co-Advisor: Edward B.Thornton

Approved for public release; distribution is unlimited.

REPORT DOCUMENTATION PAGE

Form Approved
OMB No. 0704-0188

1. AGENCY USE ONLY *(Leave blank)*	2. REPORT DATE	3. REPORT TYPE AND DATES COVERED
	June 2000	Master's Thesis

4. TITLE AND SUBTITLE Sand Bed Roughness in the Nearshore, COAST 3D Experiment, Egmond aan Zee, The Netherlands

5. FUNDING NUMBERS

6. AUTHOR(S)
Kendall, Robert L.

7. PERFORMING ORGANIZATION NAME(S) AND ADDRESS(ES)
Naval Postgraduate School
Monterey, CA 93943-5000

8. PERFORMING ORGANIZATION REPORT NUMBER

9. SPONSORING / MONITORING AGENCY NAME(S) AND ADDRESS(ES)
NSF, 4201 Wilson Blvd, Arlington, VA 22230

10. SPONSORING / MONITORING AGENCY REPORT NUMBER
9811207

11. SUPPLEMENTARY NOTES
The views expressed in this thesis are those of the author and do not reflect the official policy or position of the Department of Defense or the U.S. Government.

12a. DISTRIBUTION / AVAILABILITY STATEMENT
Approved for public release; distribution is unlimited.

12b. DISTRIBUTION CODE

13. ABSTRACT ***(maximum 200 words)*** Sand bed roughness was measured in the nearshore during a variety of hydrodynamic conditions using an array of seven 1 MHZ sonar altimeters mounted on the WESP (an amphibious vehicle used for measuring large-scale bathymetry) during the COAST 3D Experiment 1998, at Egmond aan Zee, The Netherlands. Corollary waves were modeled using the Thronton and Guza (1983) wave transformation model. Wave height and current measurements were made in the surf zone using pressure sensors and electromagnetic current meters, and offshore wave heights were measured using an advectional wave-rider buoy. Measurements of sand bed roughness showed patterns similar to those observed by Clifton et al. (1971), but are highly variable both spatially and temporally with dependence on large scale morphology and wave and current conditions. Mobility number (Ψ) calculated from the modeled wave field and also from measured currents revealed that roughness is a function of Ψ. Roughness was observed to be highly variable at low Ψ (< 100) calculated from the modeled wave heights. As Ψ increased (100-150), roughness decreased gradually, but was still highly variable. As Ψ reached values greater than 150, roughness was restricted to the lowest observed values (< 3 cm) implying planar beds under sheet flow conditions.

14. SUBJECT TERMS
Sand Bed Roughness, Megaripples, Ripples, Sediment Transport, Nearshore Processes, Morphology

15. NUMBER OF PAGES
89

16. PRICE CODE

17. SECURITY CLASSIFICATION OF REPORT	18. SECURITY CLASSIFICATION OF THIS PAGE	19. SECURITY CLASSIFI- CATION OF ABSTRACT	20. LIMITATION OF ABSTRACT
Unclassified	Unclassified	Unclassified	UL

NSN 7540-01-280-5500

Standard Form 298 (Rev. 2-89)
Prescribed by ANSI Std. 2318

Approved for public release; distribution is unlimited

SAND BED ROUGHNESS IN THE NEARSHORE, COAST 3D EXPERIMENT, THE NETHERLANDS

Robert L. Kendall
Lieutenant Commander, United States Navy
B.S., The University of Dayton, 1985
M.S., The University of Akron, 1989

Submitted in partial fulfillment of the
requirements for the degree of

MASTER OF SCIENCE IN METEOROLOGY AND PHYSICAL OCEANOGRAPHY

from the

NAVAL POSTGRADUATE SCHOOL
June 2000

Author: Robert L Kendall
Robert L. Kendall

Approved by: Edith L Gallagher
Edith L. Gallagher, Thesis Advisor

Edward B. Thornton
Edward B. Thornton, Co-Advisor

Edward B. Thornton
Roland W. Garwood, Chairman
Department of Oceanography

ABSTRACT

Sand bed roughness was measured in the nearshore during a variety of hydrodynamic conditions using an array of seven 1 MHZ sonar altimeters mounted on the WESP (an amphibious vehicle used for measuring large-scale bathymetry) during the COAST 3D Experiment 1998, at Egmond aan Zee, The Netherlands. Corollary waves were modeled using the Thronton and Guza (1983) wave transformation model. Wave height and current measurements were made in the surf zone using pressure sensors and electromagnetic current meters, and offshore wave heights were measured using an advectional wave-rider buoy. Measurements of sand bed roughness showed patterns similar to those observed by Clifton et al. (1971), but are highly variable both spatially and temporally with dependence on large scale morphology and wave and current conditions. Mobility number (Ψ) calculated from the modeled wave field and also from measured currents revealed that roughness is a function of Ψ. Roughness was observed to be highly variable at low Ψ (< 100) calculated from the modeled wave heights. As Ψ increased (100-150), roughness decreased gradually, but was still highly variable. As Ψ reached values greater than 150, roughness was restricted to the lowest observed values (< 3 cm) implying planar beds under sheet flow conditions.

TABLE OF CONTENTS

ACKNOWLEDGMENT

I would like to thank my thesis advisors, Professor Edie Gallagher and Professor Ed Thornton, for their instruction, guidance, which has made this study possible. Their exceptional professional advice, patience, and support were invaluable.

This study would have not been accomplished if it was not for the scientific and technical expertise of several individuals: Mark Orzech for his programming assistance; LCDR Bruce Morris for his model code and his Naval camaraderie, and Dr. Ad Reniers for his scientific expertise.

I would also like to thank my parents for their support of all of my education and my Naval career.

Above all, I could not have accomplished this study without the love and support of my wife Robin and two children, J.W. and Kimberlee. I could not have finished this study without their patience, flexibility, and encouragement. Thank you all!

I. INTRODUCTON

Barred beaches are composed of highly variable and complex bedforms (Clifton et al., 1971). The formation and distribution (spatial and temporal) of these bedforms is poorly understood, and a better understanding would be a valuable tool for determining bottom friction and resulting wave energy dissipation, current generation in the nearshore, sediment transport and resulting bathymetry changes, as well as for interpretating paleo-environments.

Significant information is available on small-scale morphology in steady unidirectional currents, e.g. rivers and estuaries (Middleton and Southward, 1984, Fredsoe and Deigaard, 1992). In general, bed state is separated into different regimes (e.g., ripples, flatbed, etc.) which are a function of flow strength, flow depth and grain size. Similarly, Clifton et al. (1971) described the spacially varying bedforms on a non-barred beach in terms of flow regimes (Fig. 1). They observed that well outside the surf zone the bed is dominated by straight asymmetric ripples, 2–5 cm high, with 10–20 cm wavelengths. Immediately seaward of the breaker line in the zone of wave build-up, they described the occurrence of landward-oriented lunate megaripples (30–100 cm high, 1–5 m long). Beneath the breakers they observed a planar bed. The inner portion of the surf zone is characterized by large-scale, long-crested, symmetric ripples described as having heights of 15–20 cm and lengths of 30–60 cm, as well as large megaripples. Planar beds characterized the swash zone. Clifton et al. (1971) suggested that this landward sequence

is the result of an increase in flow regime associated with a shoreward increase in orbital velocity and velocity asymmetry at the bottom.

Clifton (1976) developed a conceptual bedform model based on maximum bottom orbital velocity, velocity asymmetry, median grain size and wave period, which consists of four main regimes including no sediment flow, symmetric bedforms, asymmetric bedforms and flat bed (sheet flow). Davidson-Arnott and Greenwood (1974) also studied bedforms on a barred beach and developed a basic regime model which divides each bar and trough into four subregions, and corresponding flow regimes analogous to Clifton (1976).

These studies employed SCUBA to observe bedforms in situ and therefore were conducted during relative calm conditions. During storms, the turbulent environment of the nearshore is impassable, thus observations during high energy conditions were impossible. More recently, acoustics have been used. For example, stationary sonar altimeters have been used to investigate bedforms in the nearshore (Dingler and Clifton, 1984, Hay and Wilson, 1993) and to measure accretion and erosion in the surf zone (Gallagher et al., 1998) and in intermediate water depth (8 m) (Wright et al., 1986). Dingler and Inman (1976), Dingler and Clifton (1984), and Greenwood et al. (1993) used a track-mounted vertical sounder to obtain 2-D profiles of bed elevation at a single location inside the surf zone. Hay and Wilson (1994) used a rotary sidescan sonar to document the continuous evolution of bedforms through time over a 10 m^2 area on the crest of a nearshore bar where they observed the occurrence of ripples, cross ripples, megaripples, and transition between ripple types during the waning stages of the storm.

Thornton et al. (1997) measured small-scale morphology related to wave and current parameters across the surf zone using a single altimeter mounted on an amphibious surveying vehicle. Gallagher et al. (2000) made similar measurements with an array of seven sonar altimeters mounted on the same moving platform to characterize the sand bed roughness in the nearshore over a 500 m X 700 m area. Here similar measurements of bedforms for a different beach are presented. In Chapter II the experiment is described, and in Chapter III analysis techniques will be documented. In Chapter IV, the observations will be presented, and in Chapter V they will be discussed. The objective of this study is to characterize sand bed roughness and its spatial and temporal variability in the nearshore, and to quantify the degree of roughness by comparing to wave conditions.

THIS PAGE INTENTIONALLY LEFT BLANK

II. COAST 3D EXPERIMENT

The data presented were obtained as part of COAST 3D, a comprehensive nearshore field experiment (Mulder, 1997) conducted over a six-week period in October-November 1998 at Egmond aan Zee, the Netherlands (Fig. 2). The objective of the study described here was to measure the spatial and temporal distribution and variability of bedforms in the nearshore under a wide variety of conditions.

The WESP, a 15 m high, amphibious, motorized, three-wheeled vehicle made daily surveys of the large-scale bathymetry (e.g. sand bars) using DGPS (Fig. 3). An example of a two-dimensional bathemetric contour map produced from the data collected by the WESP describing the large-scale morphology is shown in Figure 4. The vertical and horizontal error of the WESP bathemetric surveys is estimated at 10 cm (Ruessink et al., submitted), and the alongshore separation of the survey lines was about 50 m. Bathymetry measured by the WESP was sampled at approximately 1 Hz, (although the data were not evenly spaced in time). The spatial separation of data is dependent on the speed of the WESP. The WESP speed is O(1 m/s) resulting in a cross-shore resolution of O(1 m).

The elevation of the small-scale morphology, which the WESP cannot resolve, was measured using an array of 7, 1 MHz sonar altimeters attached to the rear of the WESP (Fig. 5) following the methods of Gallagher et al (1996), Thornton et al. (1997), and Gallagher et al. (2000). The altimeters were sampled at 48 Hz so the cross-shore resolution (also dependent on WESP speed) is O(2 cm). The altimeters have a much higher vertical resolution O(mm) than does the WESP DGPS, and the closest spacing

between altimeters is 15 cm. The data were corrected for pitch, roll and yaw of the WESP using measured heading and tilts. The cross-shore profiles produced using the altimeters are closely spaced with vertical resolution of about 3 cm (Gallagher et al., 1998) and cross-shore resolution of about 5 cm and alongshore resolution of about 40 cm. Thus altimeters are capable of measuring the small-scale bedforms (i.e., large ripples and megaripples).

The field site forms part of the 120 km long uninterrupted Holland coast and faces the North Sea. The nearshore subtidal morphology is characterized by a shore-parallel double sandbar system with a mean slope of 1:100 (Ruessink et al., 2000). Sediments at the field experiment near Egmond are well sorted and composed of fine to medium sand with a mean grain size between 0.25 and 0.35 mm (Krone et al., 1997). The inner bar often contains significant quasi-periodic alongshore variations with a wavelength varying between 350 and 900 m (Ruessink et al., 2000). The outer bar can be described as being either straight or containing rhythmic features with length scales of more than 1 km (Ruessink et al., 2000).

Offshore wave conditions (Table1, Fig. 6) were acquired from an advectional wave rider buoy located approximately 5 km offshore in 16 m water depth. The first 14 days of the COAST 3D field experiment were characterized by an increase in significant wave height, $H_{1/3}$, from 1 to 3 m (Fig. 6a). During the next six days, large waves ($H_{1/3}$ = 2-5.5 m) were observed. Afterwards, the offshore wave conditions decreased considerably with the exception of day 26. Significant wave period, $T_{1/3}$, ranged from 3 to 10 s (Fig 6b), mimicking the development of the $H_{1/3}$. Wave directions during the experiment were from the southwest (-45°) or from the northwest (+45°) (Fig. 6c). The

tide is semi-diurnal with a mean range of 1.5 m. Storm surge levels periodically raised water levels by more than 1 m causing low-water levels to be higher than ordinary flood levels (Ruessink et al., 2000). Figure 6d is offshore water level measure in NAP, Dutch ordnance level.

THIS PAGE INTENTIONALLY LEFT BLANK

III. METHODOLOGY

The WESP survey and altimeter measurements were combined to obtain highly resolved bottom profiles at the Egmond field site during the COAST 3D Experiment (Fig. 7). GPS data were linearly interpolated to 48 Hz and a median filter was used to remove bad returns from the altimeter data (Thornton et al., 1997). After correcting altimeters for pitch, roll and yaw, profiles of cross-shore distance versus WESP survey depth plus height from the bed to the altimeters were obtained (Fig 7a). Cross-shore profiles of bedforms only were generated by subtracting smoothed WESP profiles of the large scale bathymetry.

This study will focus on the root mean square (RMS) roughness of the seafloor after the method of Gallagher et al. (2000), although the array is capable of resolving cross- and alongshore wavelengths of bedforms. Cross-shore profiles RMS of roughness are calculated using demeaned, 80 % overlapping, 25 m-long sections of the bedform profile. For each survey grid line, the seven roughness profiles (one from each sonar) are averaged to give a single roughness profile (Fig. 7). Thus, for each daily WESP survey, which consisted of 20 grid lines (10 grid lines for a small survey), a map of RMS roughness is generated (see for example Fig. 8). In Figure 8, the map of roughness is overlain by contours of large-scale bathymetry measured by the WESP.

Bad RMS roughness values were removed from the profiles prior to mapping. Roughness points were determined to be bad if a particular point was not consistent with surrounding points, e.g., if a point was > 1.5 time the surrounding points it was considered anomalous (this threshold was found by trial and error). Also, roughness points were sometimes anomalous owing to aliasing of rapid changes is large-scale

morphology. For example, a steep slope on a sand bar was poorly resolved by the WESP, and not properly filtered as a large-scale feature. Thus the bar was included in estimates of bedform roughness. (Better filtering techniques could correct this aliasing problem.) Each roughness profile was compared to its corresponding bedform-only profile and cross-shore depth profile, and any bad points were removed.

IV. OBSERVATION

The RMS roughness (here on referred to as "roughness") patterns in the nearshore are overlain by bathymetry contours in Figures 8-14. The typical pattern (e.g. Fig. 11, $H_{1/3}$=0.98 m) consists of roughness on the shoreward slope of the outer bar with the outer trough characterized by less roughness. Roughness increases again on the seaward face of the inner bar and is greater than that observed along the shoreward face of the outer bar. Roughness decreases near the crest of the inner bar and increases again shoreward of the inner bar.

However, observed patterns of roughness in the shallow water are highly variable. For example, a short survey (500 m by 300 m, Fig. 12, $H_{1/3}$=0.7 m) revealed significant roughness on the crest of the inner bar and a relatively smooth bed on the seaward slope of the bar. Although this survey does not cover the whole area, the variation from the above pattern can be seen. In addition, breaks in the inner bar, possibly owing to rip currents, show areas of anomalously high roughness (Fig. 11, Fig. 13, and Fig. 14). High roughness in rip current channels has been observed by Thornton et al (1997) and Vincent and Osbourne (1993).

The typical roughness patterns observed during this study are analogous to Clifton's (1976) observations (Fig. 1). His conceptual model shows the transitions of small-scale morphology from wave ripples to megaripples on the seaward slope of the bar, to a planar bar crest due to the increase in wave intensity, and to wave or megaripples again in the trough where wave intensity decreases after waves have crossed the bars.

This general sequence of bedforms with increasing flow strength described by Clifton (1976), and observed by others (e.g. Davidson-Arnott and Greenwood, 1976, Hay and Wilson, 1994, Thornton et al., 1997, and Gallagher, 2000) is:

no movement – ripples (small) – megaripples – plane bed.

This sequence is typical for fine sand (<0.2 mm) (Davidson-Arnott and Greenwood, 1976). Davidson-Arnott and Greenwood (1976) observed that as grain diameter increases, the occurance of megaripples increases, and that of ripples decreases until coarse sand (1.0 mm and greater) when ripples are no longer formed and the sequence becomes:

no movement – plane bed – megaripples – plane bed.

There have been variations reported on these typical bedform sequences. For example, Southard and Boguchwal (1973) have shown that there is a transitional area between fine and coarse sand in which the succession of bedforms is more complex:

no movement – ripples – plane bed – megaripples – upper flat bed.

The bedform sequence observed at Egmond, where median grain size is 0.3 mm, appears to be typical for fine sand. For example, typical cross-shore transects are found in Figures 15-19. (Example transects are taken from alongshore location y=775 m because they are co-located with the pressure and current measurements, see section V.) On these days, roughness is low (<5 cm) on the crest of the outer bar where waves are shoaling, and possibly breaking, suggesting planar bed under sheet flow conditions (Fig. 15d,e and 19d,e). As water depth increases over the shoreward face of the outer bar and trough, roughness increases (5-12 cm) but decreases again (< 5 cm) in the outer trough. An increase in roughness (7-10 cm) is seen as water depth decreases again on the seaward

face of the inner bar. Along the crest of the inner bar, a decrease in roughness is seen owing to increased flow strength as waves break, perhaps generating sheet flow or small ripples. The inner trough is characterized by large, but highly variable roughness, what Clifton (1976) called the "inner rough" regime, probably owing to the complex flow field in the inner surf zone (Fig. 16d and 19d).

While the above examples show striking similarities to the Clifton (1976) bedform distribution sequence, there are variations that deserve attention. For example, during the highest waves of the experiment, (Table 1, Fig. 18c) the crests of the bars are planed off as well as the bar slopes, and in the troughs the roughness is very high (8-12 cm) indicating megaripples. There appears to be little or no transition down to what may be analogous to small ripples associated with a low flow regime.

Another variant on the bedform sequence conceptual model (Clifton, 1976) is the effect of steady currents (longshore, tidal, rips) on roughness. Between 24 October and 8 November, there were a series of storms, which cut rip current channels through the inner bar (Fig. 13 and Fig. 14). Roughness in the rip channels (Fig. 13, y=775 m and Fig.14, y=700 m) is noticeably higher (5-8 cm) compared to the roughness (< 5 cm) on the adjacent bar crests to the north and south. The dominant process controlling bedform generation and movement in the rips is most likely the unidirectional current, and wave oscillatory currents are of lesser significance (Davidson-Arnott and Greenwood, 1976). Bedforms generated by combined wave-current flows occur in many coastal sub-environments, and Nielson (1992) observed that in shallow bar troughs, or rip feeder channels, conditions are current-dominated, with bedforms resembling current dunes.

Thornton et al. (1997) observed seaward facing lunate and straight-crested megaripples at Duck, NC suggesting that the offshore rip current dominated bedform processes over the oscillatory wave-generated flow.

V. Discussion

Clifton (1976) hypothesized that different bed form regimes are caused by variations in the velocity field as a function of wave transformation and breaking across the surf zone. To investigate the relationship between the roughness and the wave field, wave height changes were modeled across all survey lines using the model of Thornton and Guza (1983). The wave height transformation model was initialized using input of hourly averaged RMS wave height (H_{rms}), peak frequency and mean direction measured at a wave rider buoy in 16 m of water. The model has two free parameters, B and γ_b corresponding to the intensity of wave breaking and breaking waves criterion, which were calibrated using H_{rms} values measured by the array of pressure sensors across the inner bar (Fig. 15a-19a) and agree well with values found in the literature (Thornton and Guza, 1983).

Predicted H_{rms} versus cross-shore distance (at alongshore location y=775 m) are shown in Figures 15a-19a, and the comparison with measured H_{rms} (asterisks) is good. The predicted cross-shore values of $\gamma=H_{rms}/h$ (h=depth) are shown in Figures 15b-19b to vary with the large-scale bathymetry (Fig. 15e-19e). It is hypothesized that the bed roughness is related to this normalized wave height. RMS roughness is plotted versus γ for all values of the COAST 3D experiment in Figure 20, and a clear relationship between γ and roughness is not evident.

It was further hypothesized that mobility number (Ψ), a dimensionless ratio of fluid forces (lift and drag) to gravitational force on sediment particles under waves, is a function of roughness. Nielsen (1992) summarized Ψ for waves alone,

$$\Psi = \frac{(u_{rms_b})^2}{(s-1)gd}$$

where u_{rmsb} is the rms wave induced velocity at the bottom, s is the specific gravity of quartz, g is acceleration due to gravity, and d is grain diameter (0.3 mm). The RMS wave induced bottom velocity is calculated from linear theory

$$u_{rms_b} = \sqrt{2}\frac{H_{rms}}{2}\frac{\omega}{\sinh kh}$$

where H_{rms} is the wave height calculated from the Thornton and Guza (1983) model, and k is wavenumber. It is pointed out that the $\sqrt{2}$ is due to relating the $H_{rms}= \sqrt{8}u_{rms}$ as calculated assuming a Rayleigh wave height distribution. Wavenumber is related to radial wave frequency (ω) using the dispersion relationship from linear wave theory,

$$\omega^2 = gk \tanh kh.$$

Mobility number calculated in this way is shown in Figures 15c-19c and, like γ, shows a strong relationship with the large-scale morphology. The relationship between Ψ and RMS roughness is shown in Figure 21. As found by Dingler and Inman (1976), a decrease ripple height (roughness) corresponds to higher Ψ. However at lower Ψ the bed roughness is highly variable.

Sediment movement is initialized when the critical shields parameter (θ_c) is exceeded. The Shield's parameter (θ) is given by

$$\theta = f_w \Psi$$

where f_w is an empirical wave friction factor (f_w=0.1 is a conservative estimate), and Ψ is mobility number as defined above. The critical Shield's parameter (θ_c) was calculated to be 0.4 in this study using the method of Komar and Miller (1973). Based on our calculations, θ_c was always exceeded during this experiment.

Nielsen (1981) summarized the results of wave ripple measurements in the field (Inman, 1957; Dingler, 1974; Miller and Komar, 1980) relating ripple wavelength (λ) and wave orbital excursion amplitude, a, to mobility number. Nielsen (1981) suggested for values of Ψ greater than 200, λ/a becomes minimal, implying that ripples are planed off. Dingler (1974) suggested, based on field observations, that ripples are planed off when Ψ reaches a value of 240, when considering sediments of almost entirely quartz sand. Nielsen (1981) also found that where sediments have densities close to that of quartz, it is reasonable to expect relative ripple height (η/a) to be a function of Ψ as well. Nielsen (1981) suggested that relative ripple height goes to zero for Ψ>156.

In this study, as Ψ increased to its highest values (>150), roughness is limited to the lowest observed values (< 3 cm, Fig. 21), which generally agrees with the thresholds for planar bed proposed by Dingler (1974) and Nielsen (1981). The roughness is highly

variable throughout a wide range of Ψ, and in general the roughness decreases with increasing Ψ. The highest roughness values are typically observed where $\Psi<100$.

Flume studies of unidirectional flow have shown that the transition from small ripples to large ripples (megaripples) is complete over a narrow range of only a few centimeters per second in flow velocity. Then, with increasing velocity, megaripples are observed to become lower and more rounded over a wide interval of flow velocities (Middleton and Southard, 1984). While it is difficult to compare unidirectional flow studies (such as rivers and estuaries) to the complex flow regime of the nearshore, perhaps the tapering off of roughness for $\Psi>100$ is analogous to the transition from megaripples to planar beds. However, no sharp transition is observed between ripples and megaripples.

Predicted Ψ is based on cross-shore oscillatory velocity only, thus any contribution to sediment mobility owing to steady currents is not considered. Using measured velocities from electromagnetic current meters (co-located with pressure sensors at asterisks on Fig. 15e-19e), total Ψ is calculated

$$\Psi = \frac{\bar{u}^2}{(s-1)gd}$$

where $\bar{u}^2 = (u_{rms} + U)^2 + V^2$ with U and V are the mean cross-shore and alongshore currents and u_{rms} is the square root of the cross-shore velocity variance. Alongshore velocity variance is assumed negligible.

The current meter-derived Ψ values are plotted against roughness measured in the vicinity of the sensors (Fig. 22). While there are only few points, a noticeable trend

exists, and Clifton's (1976) conceptual model is supported: small roughness elements (wave ripples) exist for small values of Ψ, larger bedforms exist for intermediate Ψ values. According to Nielsen (1992) and Dingler (1974), a reduction of roughness would be expected above about Ψ=200 corresponding to the transition to sheet flow. Unfortunately, no data exist for these conditions.

A mean roughness value was obtained for each day by averaging all roughness values for each day in both the along- and cross-shore direction. The same cross-shore extent was averaged for each survey, but alongshore extent was allowed to vary assuming alongshore homogeneity and cross-shore inhomogeneity. Mean roughness is plotted versus significant wave height for each day in Figure 23. Similar to purely steady flow bedform regime studies, for low energy and high energy conditions overall roughness is lower, corresponding to rippled beds or sheet flow, respectively. However for lowest wave conditions roughness variability is the highest, which is consistent with data in Figure 21. Although confidence in these average roughness values in high (Table 1), possible uncertainty (3 cm, see Chapter II) associated with these measurements makes this observation barely significant.

Grain size and grain size distribution, although important in sediment mobility, were not considered here. In most coastal environments, the general grain size distribution from offshore to onshore is fine to coarse, however grain size distribution can also change with a change in wave conditions. Because grain size affects the size or elimination of bedform regimes (Davidon-Arnott and Greenwood, 1976), including spatial and temporal distribution of sediment may be important. Grain size variation

needs to be considered in future studies of bedforms in the nearshore to help explain the observed complexity.

In addition, the assumption that the bedforms are in equilibrium with the present conditions may not be valid. Although relict ripples are unlikely in the high energy environment of the nearshore, there may be a lag between changing flow conditions and bedform development. Thus, a lag between forcing and morphology changes should also be considered in future studies.

VI. CONCLUSIONS

Sand bed roughness in the nearshore was measured in a variety of hydrodynamic conditions on a double-barred beach during the COAST 3D experiment at Egmond aan Zee, The Netherlands. The root-mean-squared (RMS) roughness was measured using an array of seven sonar altimeters mounted on the WESP. Corollary wave conditions were modeled using the Thornton and Guza (1983) wave transformation model, and pressure sensors and electromagnetic current meters in the surf zone acquired wave height and current measurements.

Sand bed roughness patterns observed in the nearshore at Egmond exhibited patterns similar to those described by Clifton et al. (1971), but were found to be highly variable (spatially and temporally). Roughness appears to be dependent on the large-scale morphology and influenced by the hydrodynamic conditions.

Mobility number Ψ was calculated from bed velocities derived from modeled wave heights using linear theory. For $\Psi > 150$, roughness was restricted to the lowest values (< 3 cm) observed during the experiment, implying the occurrence of plane beds under sheet flow conditions. These values of Ψ for when bed forms are planed off agree with those found in the literature. However, for conditions of low Ψ, roughness was shown to be highly variable. This variability could be owing to strong steady currents (rips, alongshore, tidal, etc.), which were not accounted for in the modeled mobility numbers.

Current velocity was measured with four current meters located on the inner bar. Mobility numbers calculated from the measured current velocity show that roughness has

a strong dependence on the current-derived Ψ. During periods of low Ψ, roughness was observed to be 3-5 cm, probably owing to vortex ripples. As Ψ increased, roughness increased to 5-15 cm owing to large ripples and megaripples. No data were available for $\Psi > 200$, thus the expected decrease in roughness was not observed.

Other factors are known to influence the development of sand bed roughness, but were not considered in this study. Variations in sediment composition and distribution is thought to influence sand bed features in terms of ripple wavelength, slope, and extent of ripple types. Interaction of currents, such as longshore, rip, and tidal have been shown to dominate bed form processes over that of oscillatory currents in certain areas of the nearshore. Remnant roughness, or a time lag between changing flow conditions and bed form development, were not considered during this study. Further investigation into these factors will contribute to the understanding of sand bed processes in the nearshore.

APPENDIX A. TABLE

THIS PAGE INTENTIONALLY LEFT BLANK

Day	Significant Wave Height (m)	Significant Wave Period (s)	Mean Roughness (cm)	Roughness Standard Deviation (cm)	95 % Confidence Interval (cm) (±)
19 Oct	1.8 - 2.0	6.3 - 6.4	6.0	1.7	0.05
22 Oct	2.3 - 2.4	7.2	5.7	2.7	0.08
24 Oct	4.7 - 5.2	8.6 - 9.0	4.8	0.8	0.01
06 Nov	0.7	4.8 - 5.2	-	-	-
08 Nov	0.9 - 1.4	3.8 - 5.7	5.2	0.9	0.03
15 Nov	0.7 - 1.0	5.8 - 6.5	3.5	0.6	0.01

Table 1. Offshore wave conditions and mean roughness for COAST 3D roughness surveys.

THIS PAGE INTENTIONALLY LEFT BLANK

APPENDIX B. FIGURES

THIS PAGE INTENTIONALLY LEFT BLANK

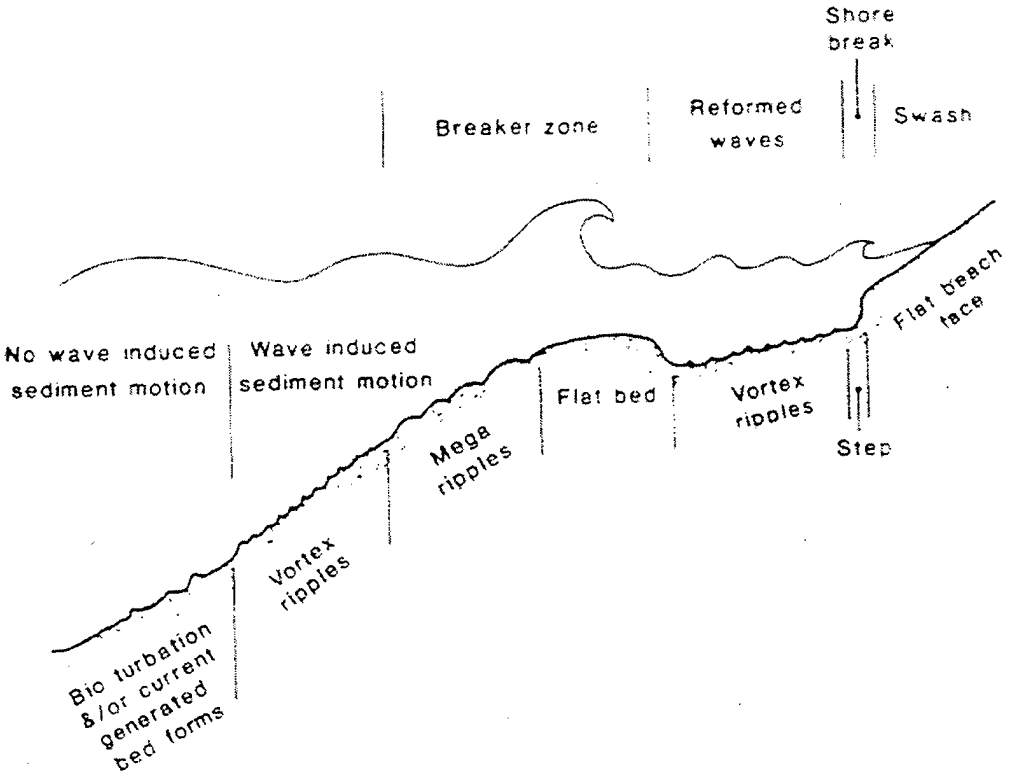

Figure 1. Distribution of small-scale morphology observed on a barred beach (from Clifton, 1976).

THIS PAGE INTENTIONALLY LEFT BLANK

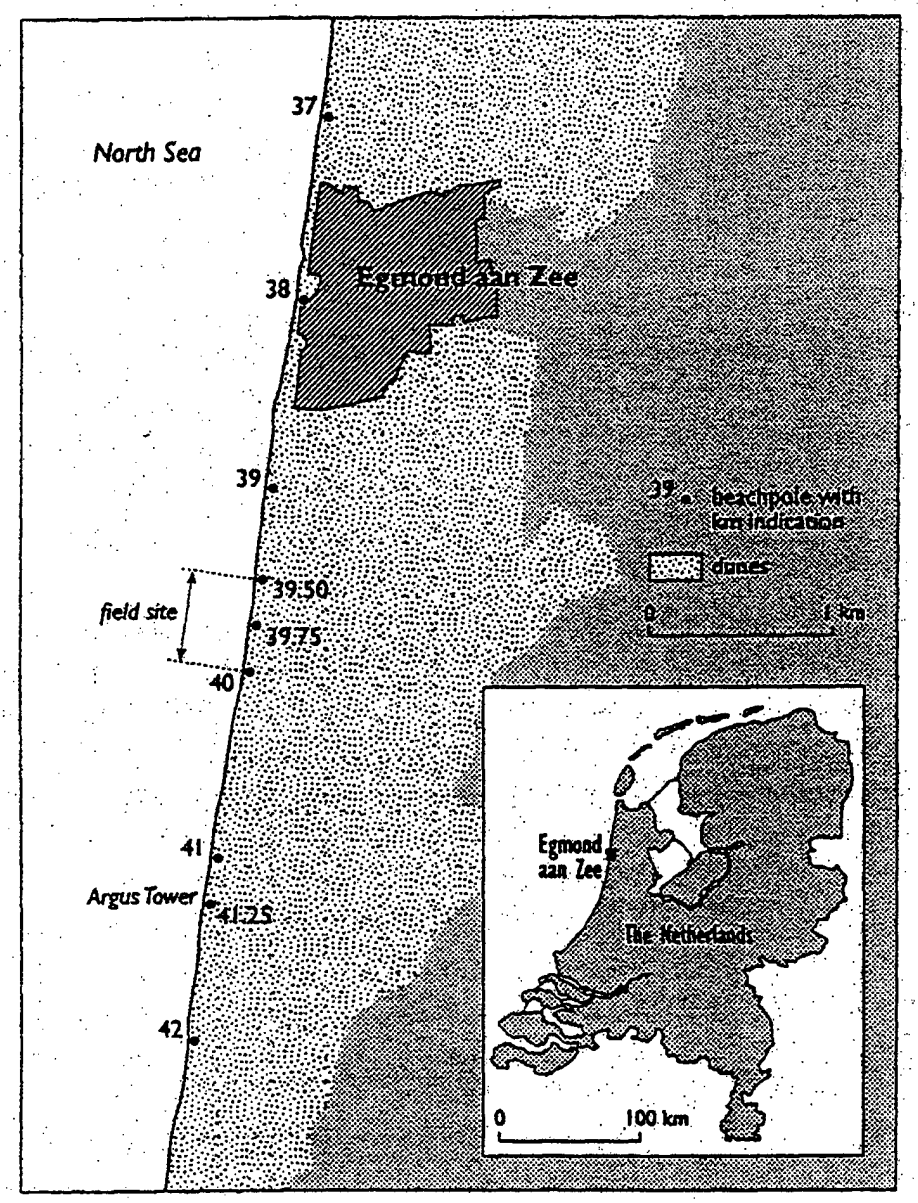

Figure 2. Map of the COAST 3D field site, Egmond aan Zee, The Netherlands (from Ruessink, 2000).

THIS PAGE INTENTIONALLY LEFT BLANK

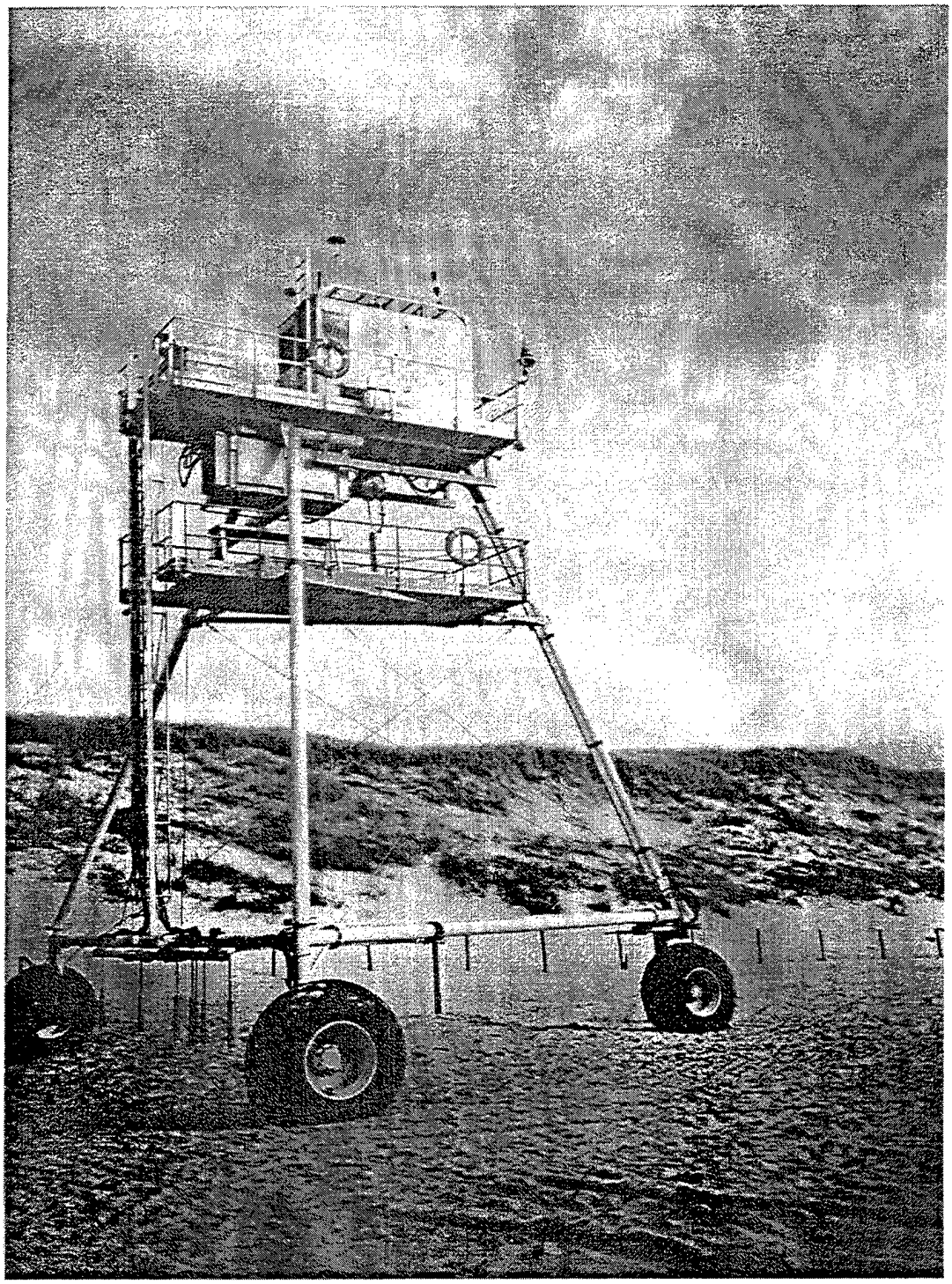

Figure 3. WESP (Water en strand Profiler) resting on the beach during COAST 3D Experiment. The WESP is about 14 m tall and 8 m wide at the rear wheels (forward is to the right), and the diameter of the tires is about 1.7 m.

THIS PAGE INTENTIONALLY LEFT BLANK

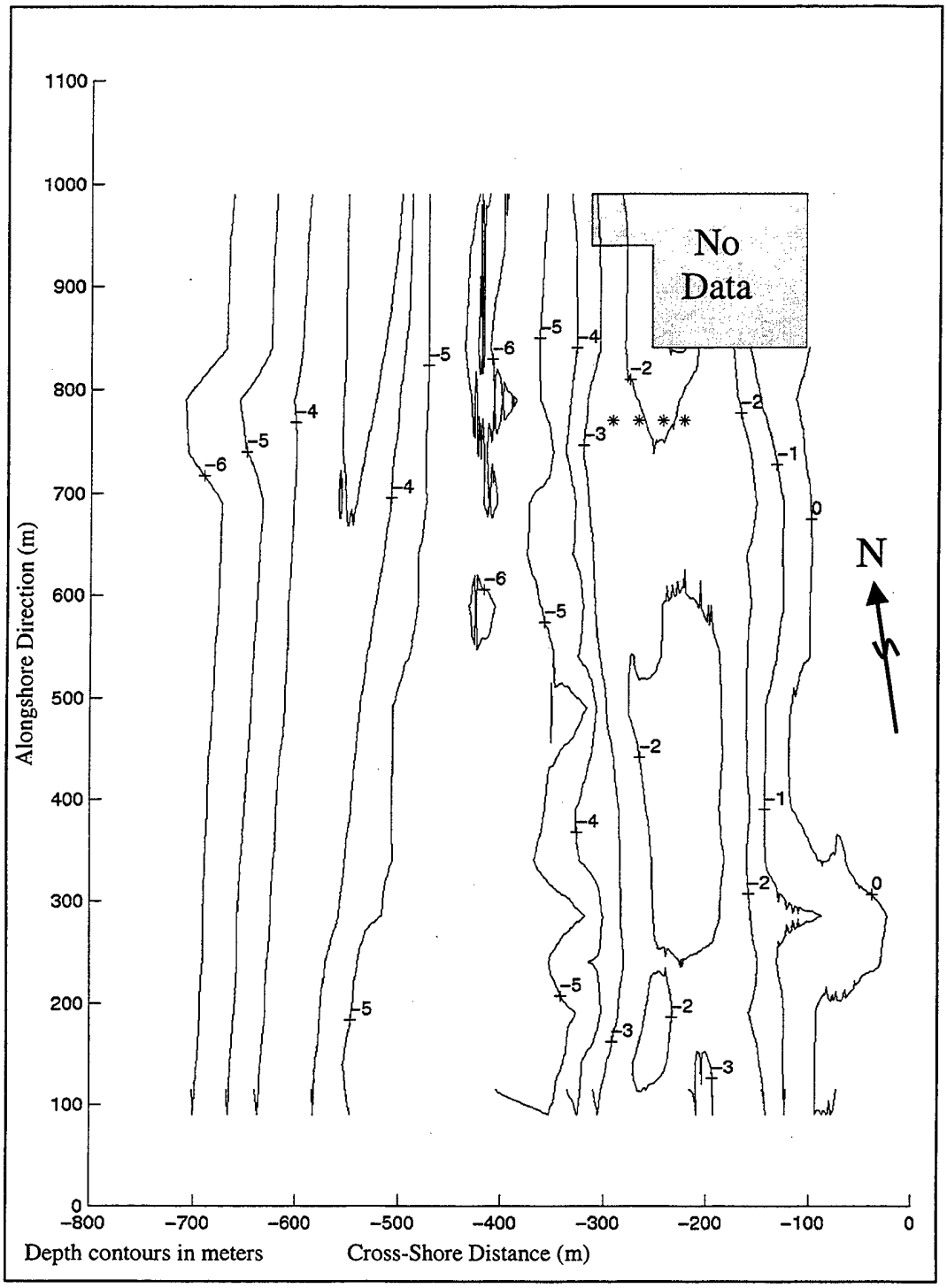

Figure 4. Example of a two-dimensional contour map produced from the data collected by the WESP on 15 November 1998. Asterisks denote the location of electromagnetic current meters and pressure sensors.

THIS PAGE INTENTIONALLY LEFT BLANK

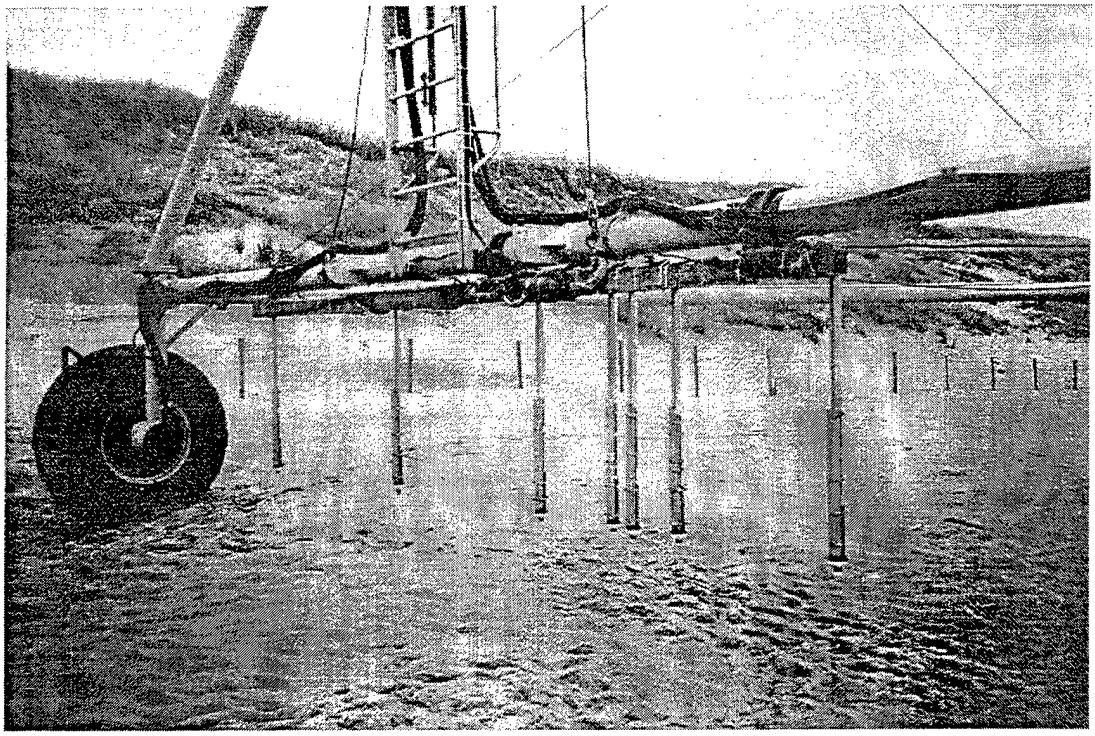

Figure 5. Close up of the array of seven sonar altimeters mounted on the rear cross member of the WESP (Fig. 3). The sonar transducers are about 70 cm above the sand.

THIS PAGE INTENTIONALLY LEFT BLANK

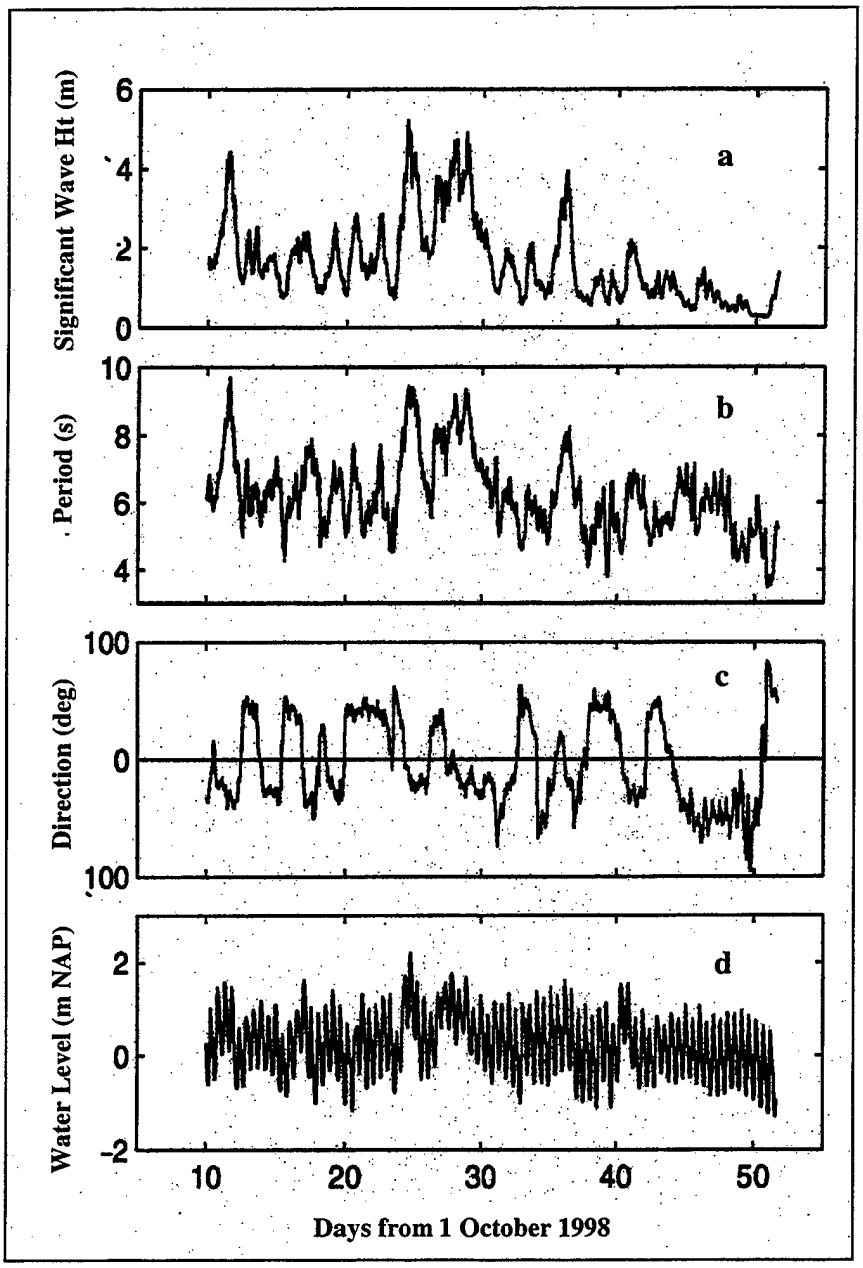

Figure 6. Offshore wave conditions during the COAST 3D Experiment. a) significant wave height. b) significant wave period. c) wave direction. d) offshore water level, where NAP is Dutch ordnance level.

THIS PAGE INTENTIONALLY LEFT BLANK

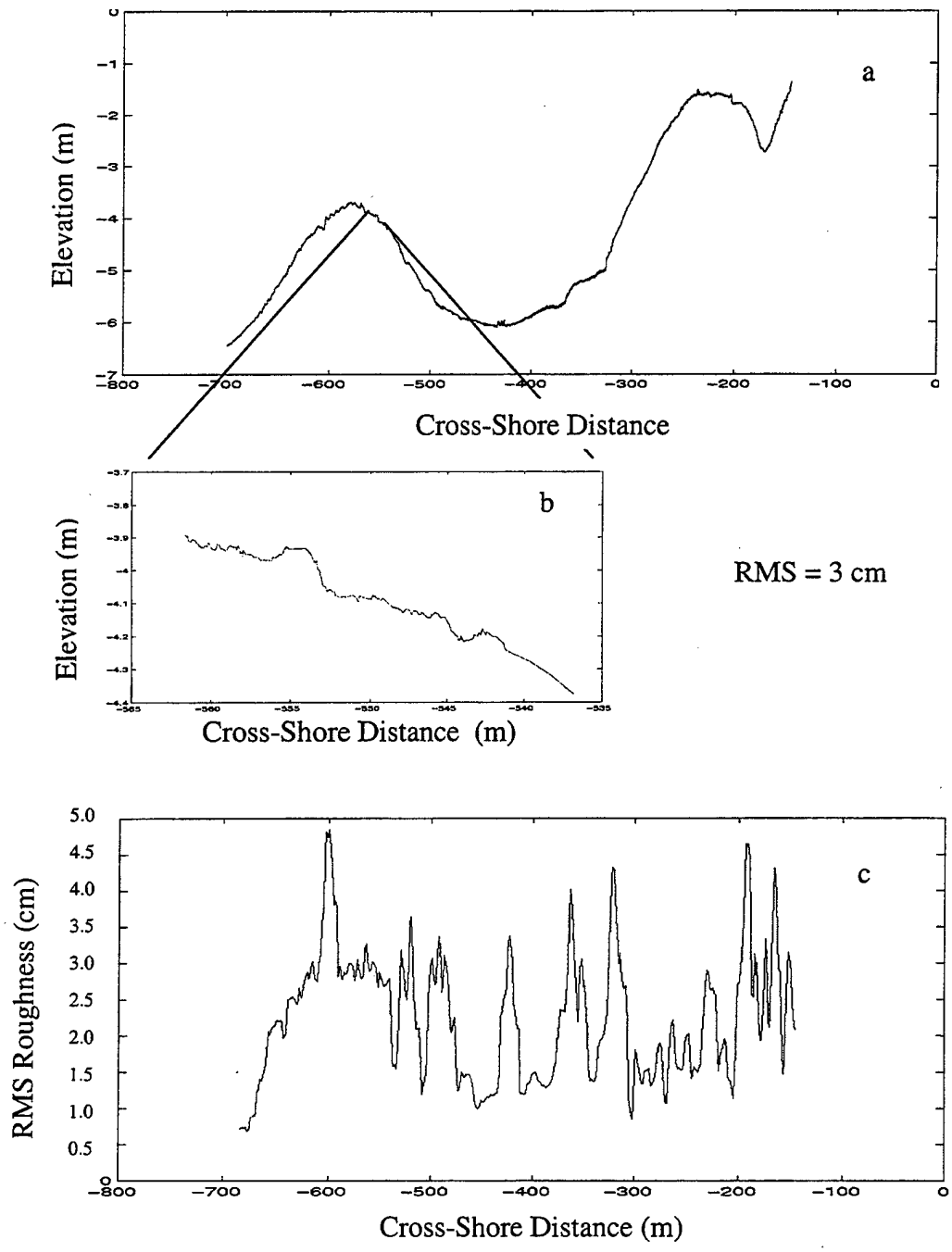

Figure 7. a) Example of a cross-shore profile from a single sonar altimeter with elevation below mean sea level vs. cross-shore distance. b) Example of 25 m-long piece of Fig. 7a. These data are detrended, and the root-mean-squared is calculated to give RMS roughness, which for this section of bedforms, is 3 cm. The RMS is calculated from overlapping sections (as in 7b), to produce this RMS roughness profile from the depth profile in Fig. 7a.

THIS PAGE INTENTIONALLY LEFT BLANK

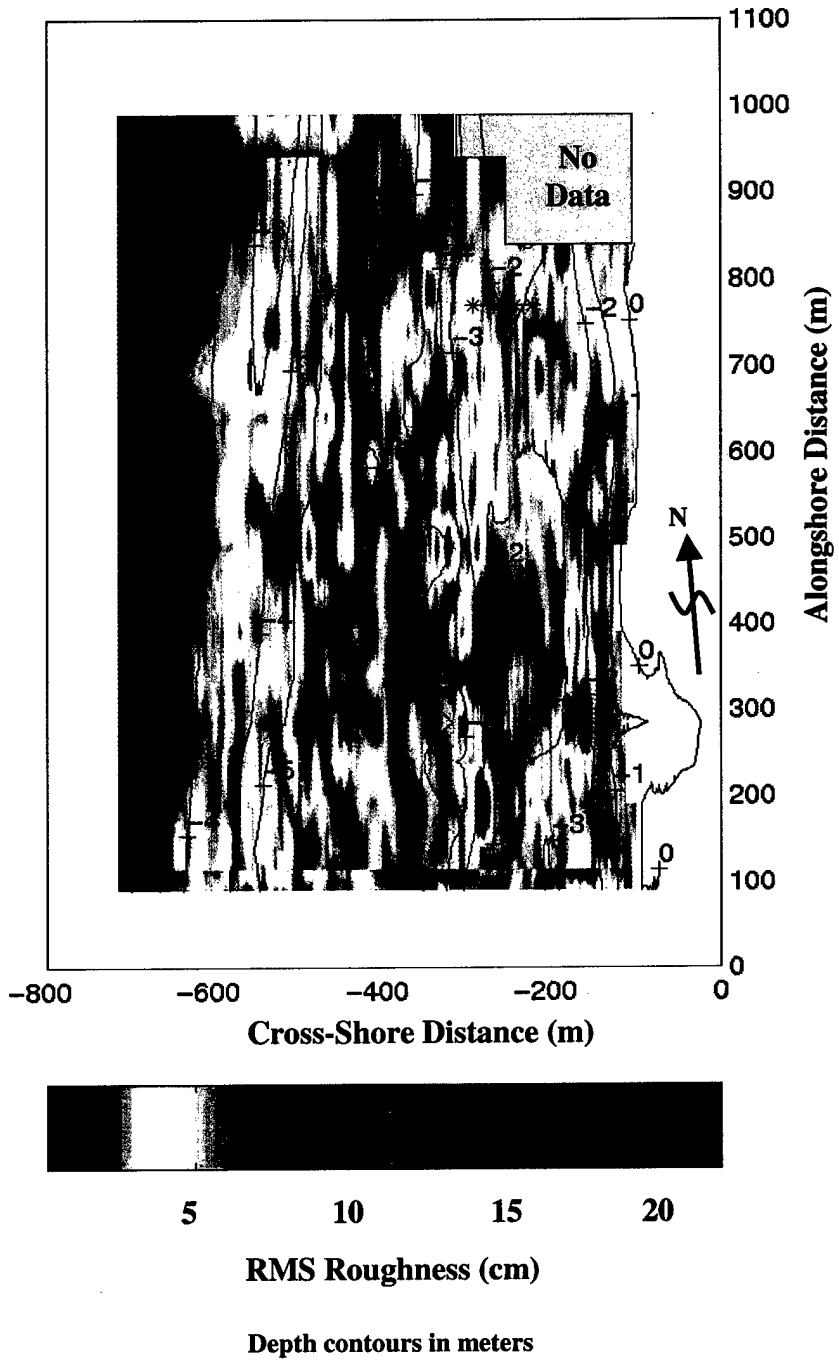

Figure 8. RMS roughness map overlain by bathymetry from data collected by the WESP for 15 Nov at the COAST 3D field site. The beach is on the right-hand side of the plot. Asterisks represent the location of current meters and pressure sensors. The cross-shore profile in Fig. 7 is take from y=500 m on this map.

THIS PAGE INTENTIONALLY LEFT BLANK

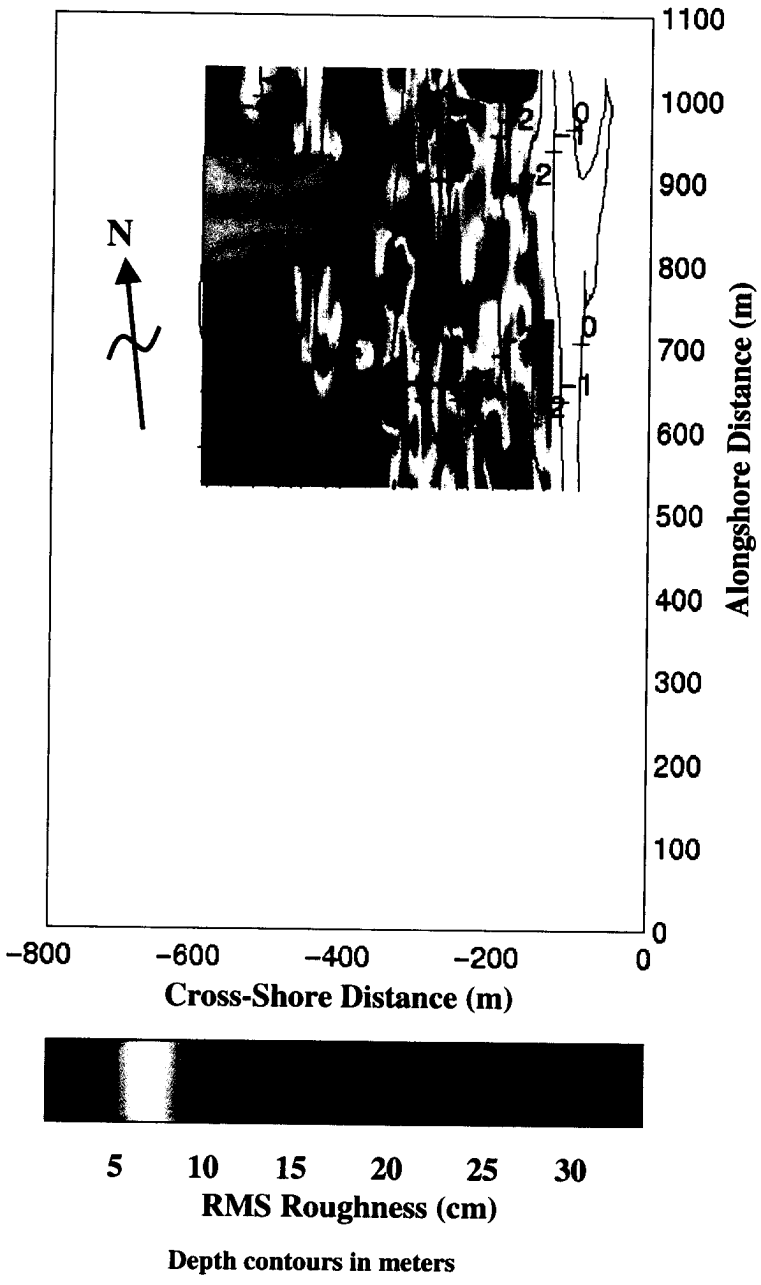

Figure 9. RMS roughness map overlain by bathymetry from data collected by the WESP for 19 Oct. at the COAST 3D field site. The beach is on the right-hand side of the plot. Asterisks denote location of current meters and pressure sensors.

THIS PAGE INTENTIONALLY LEFT BLANK

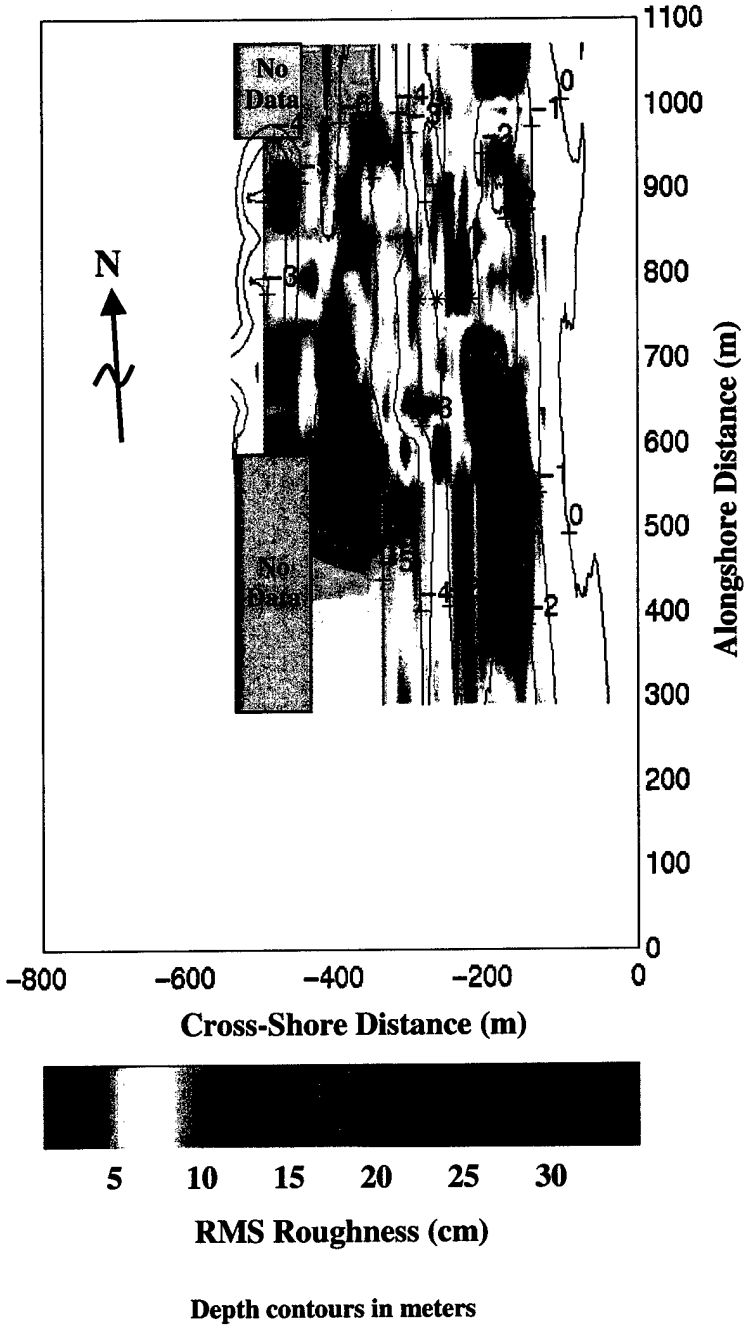

Figure 10. RMS roughness map overlain by bathymetry from data collected by the WESP for 22 Oct. at the COAST 3D field site. The beach is on the right-hand side of the plot. Asterisks denote location of current meters and pressure sensors.

THIS PAGE INTENTIONALLY LEFT BLANK

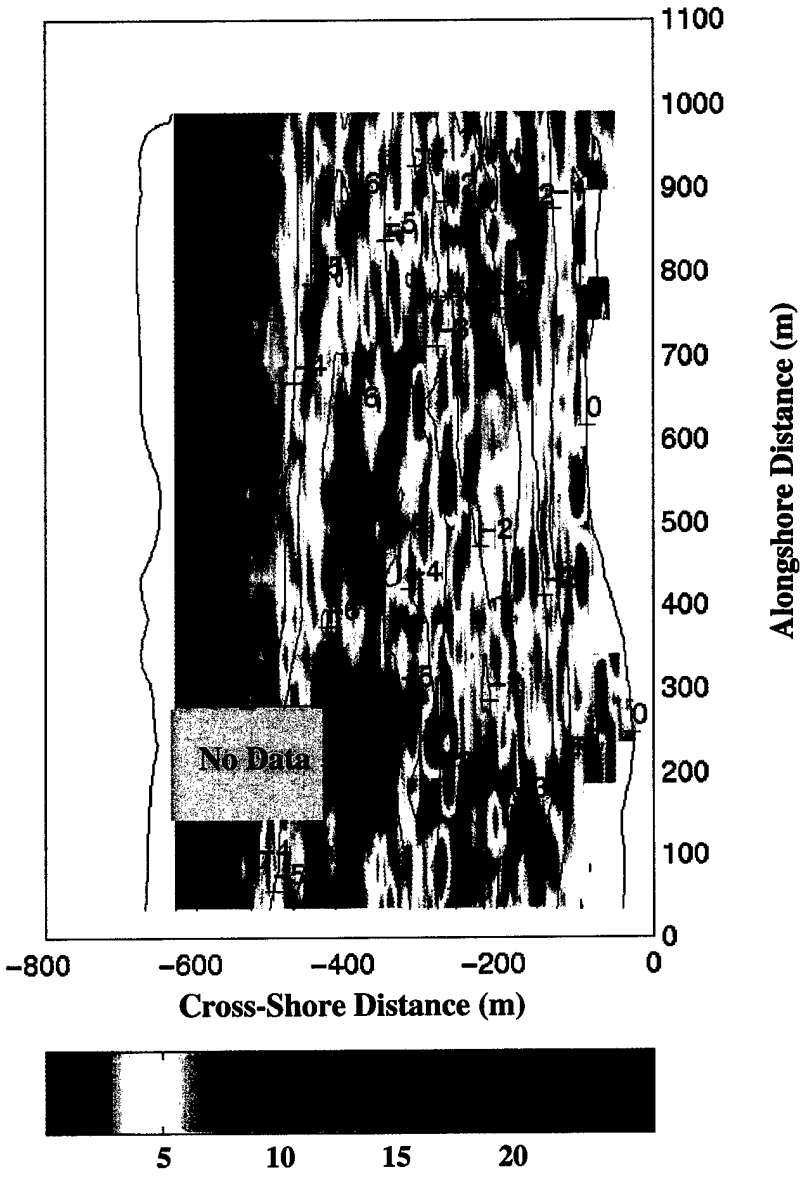

Figure 11. RMS roughness map overlain by bathymetry from data collected by the WESP for 24 Oct. at the COAST 3D field site. The beach is on the right-hand side of the plot. Asterisks denote location of current meters and pressure sensors.

THIS PAGE INTENTIONALLY LEFT BLANK

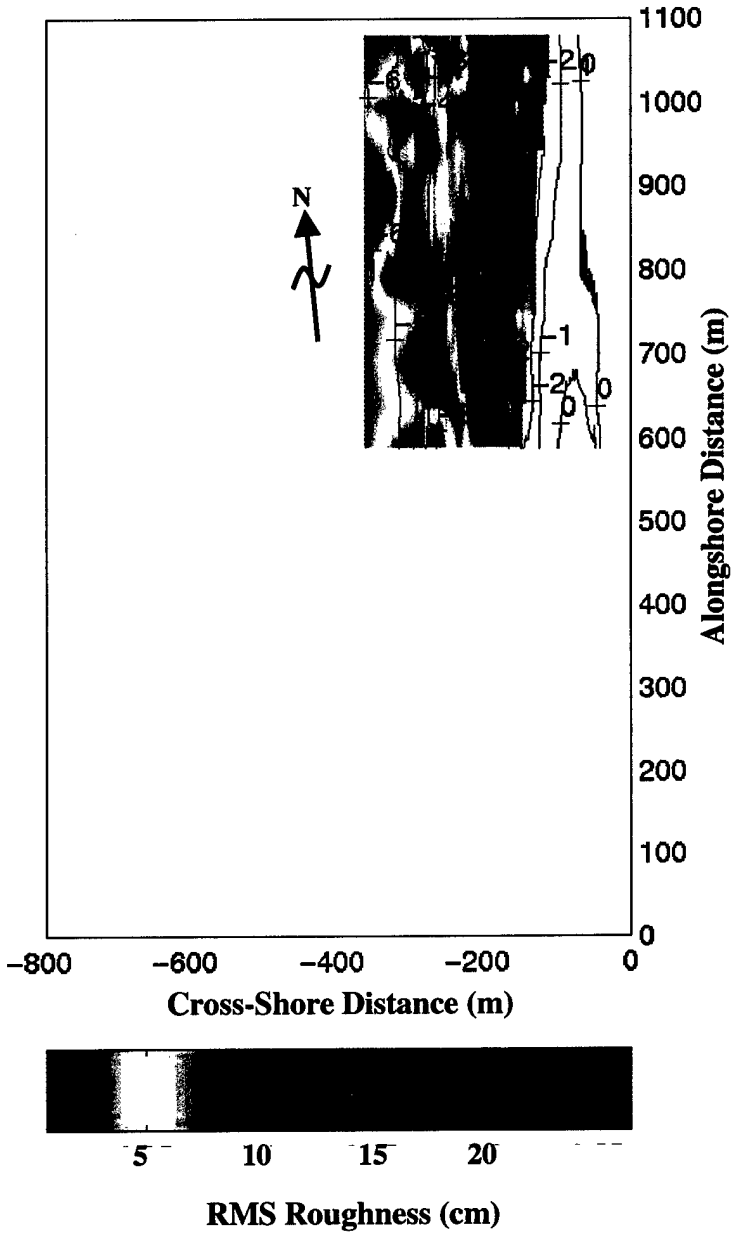

Figure 12. RMS roughness map overlain by bathymetry from data collected by the WESP for 6 Nov. at the COAST 3D field site. The beach is on the right-hand side of the plot. Asterisks denote location of current meters and pressure sensors.

THIS PAGE INTENTIONALLY LEFT BLANK

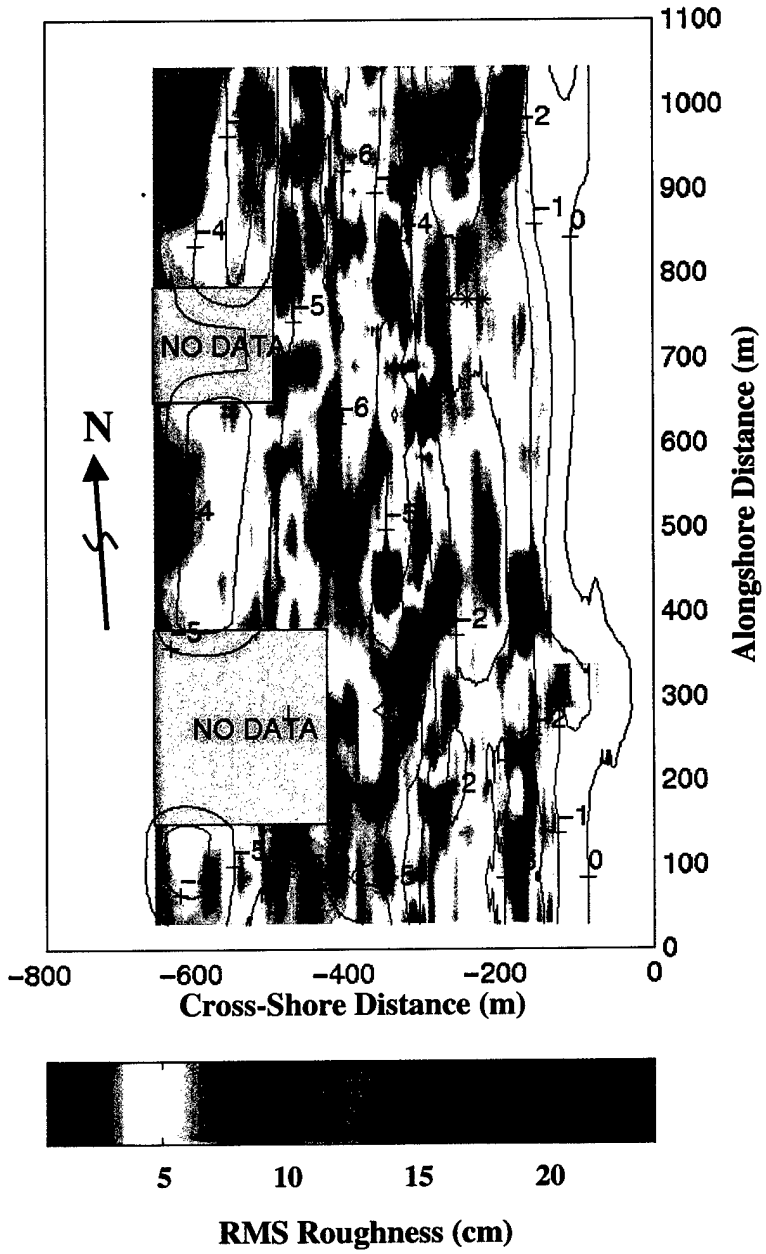

Figure 13. RMS roughness map overlain by bathymetry from data collected by the WESP for 8 Nov. at the COAST 3D field site. The beach is on the right-hand side of the plot. Asterisks denote location of current meters and pressure sensors.

THIS PAGE INTENTIONALLY LEFT BLANK

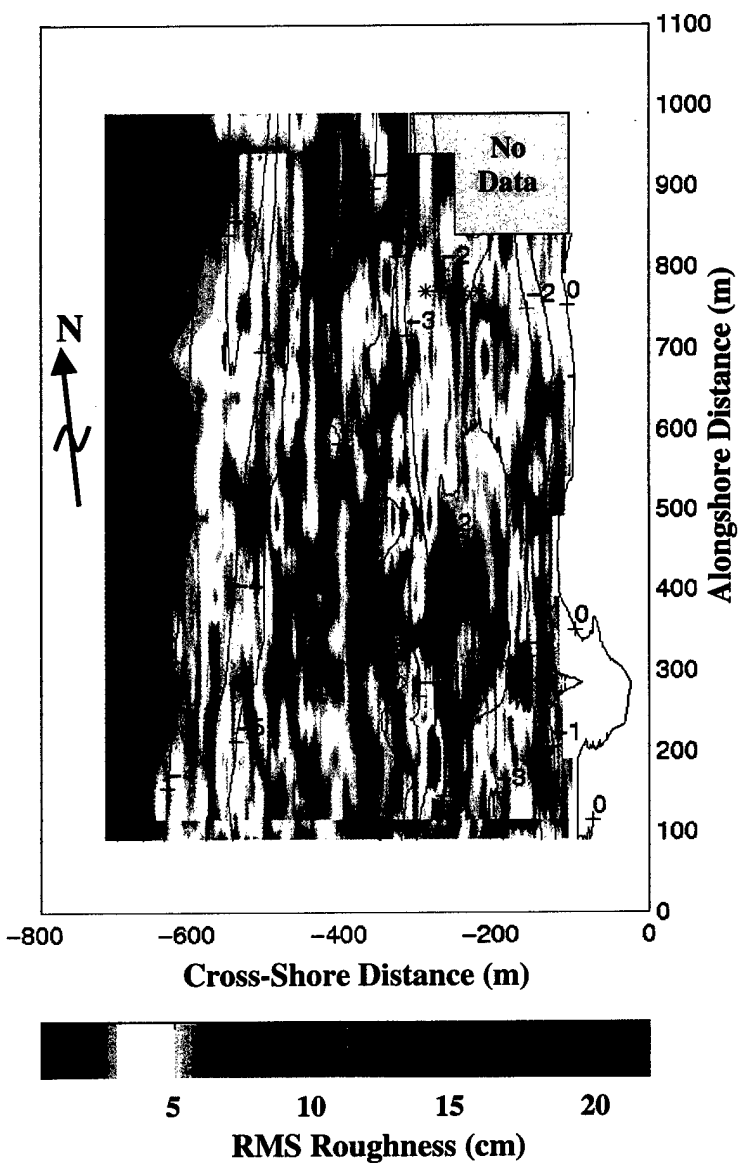

Figure 14. RMS roughness map overlain by bathymetry from data collected by the WESP for 15 Nov. at the COAST 3D field site. The beach is on the right-hand side of the plot. Asterisks denote location of current meters and pressure sensors.

THIS PAGE INTENTIONALLY LEFT BLANK

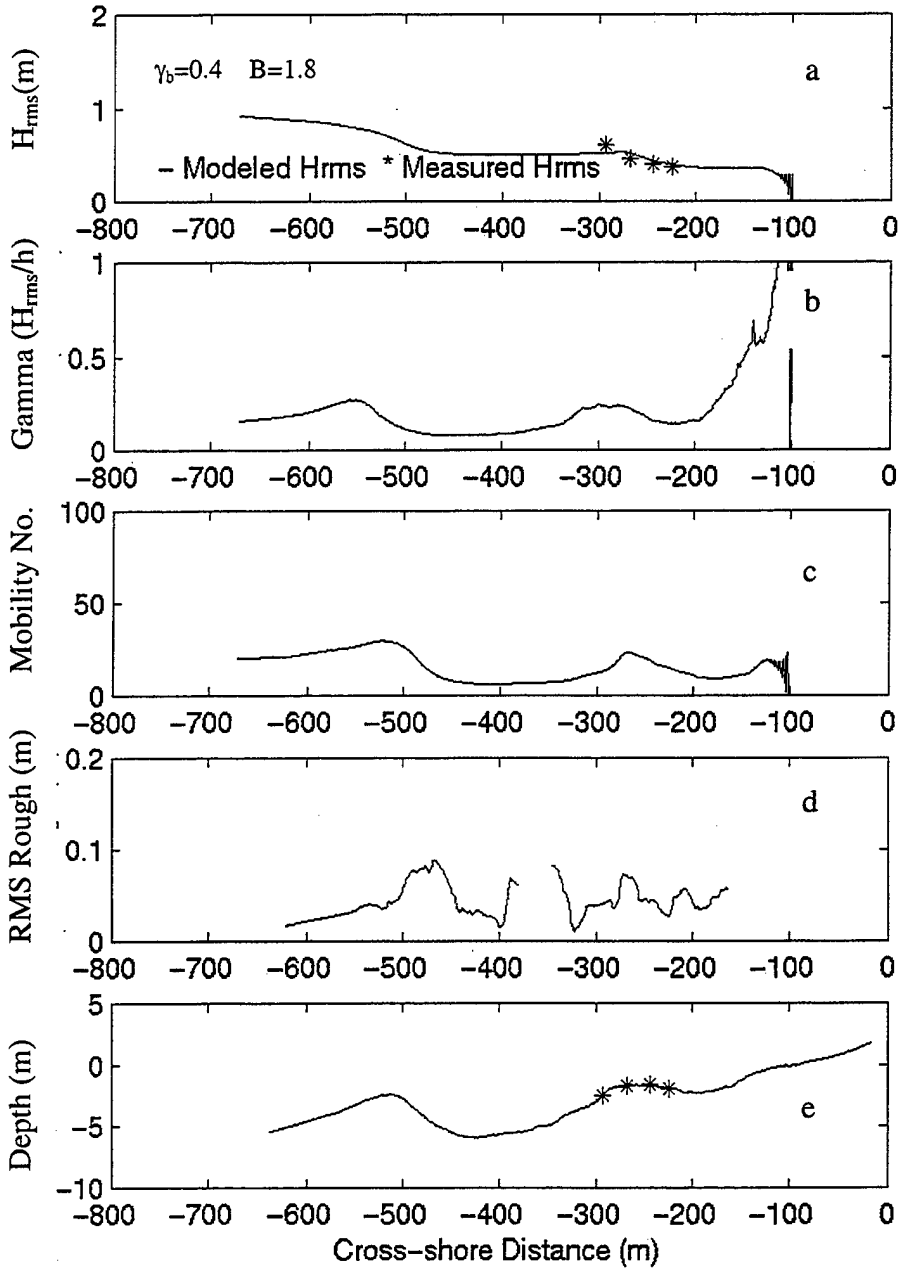

Figure 15. Cross-shore profiles for 19 Oct (at y=775 m on Fig. 9). a) modeled wave height; asterisks denote pressure meter measured wave heights. b) modeled gamma; c) mobility number calculated from modeled wave heights, d) roughness profile; and e) cross-shore depth profile, where asterisks denote location of pressure sensors and current meters.

THIS PAGE INTENTIONALLY LEFT BLANK

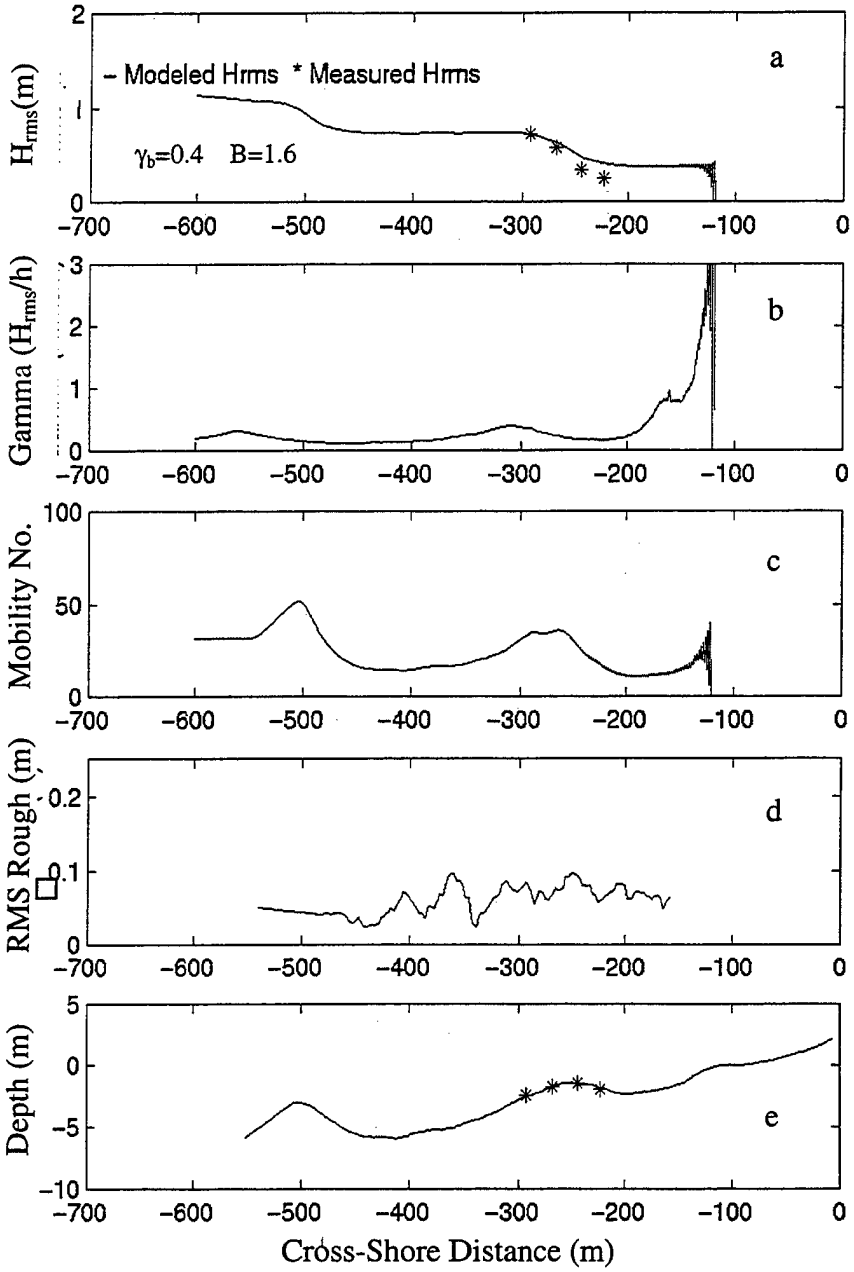

Figure 16. Cross-shore profiles for 22 Oct (at y=775 m on Fig. 10). a) modeled wave height, asterisks denote pressure meter measured wave heights. b) modeled gamma; c) mobility number calculated from modeled wave heights, d) roughness profile; and e) cross-shore depth profile, where asterisks denote location of pressure sensors and current meters.

THIS PAGE INTENTIONALLY LEFT BLANK

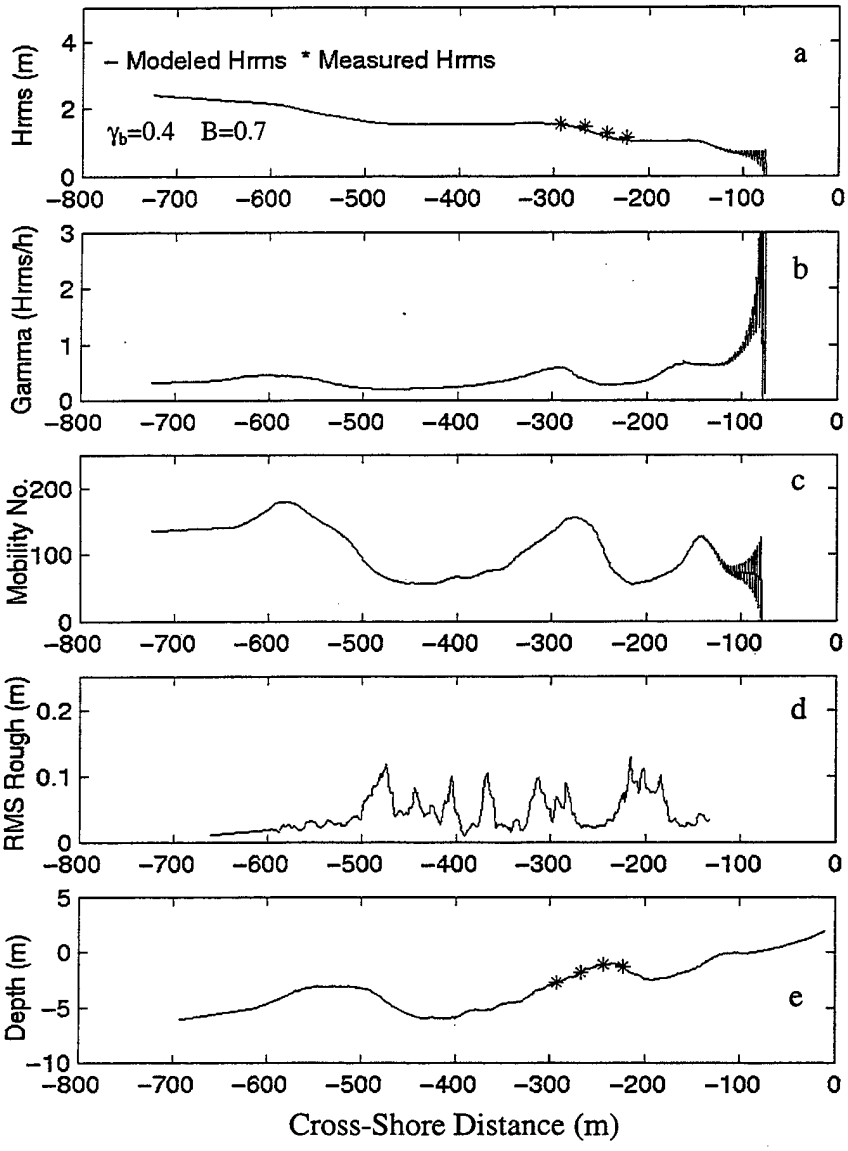

Figure 17. Cross-shore profiles for 24 Oct (at y=775 m on Fig. 11). a) modeled wave height, asterisks denote pressure meter measured wave heights. b) modeled gamma; c) mobility number calculated from modeled wave heights, d) roughness profile; and e) cross-shore depth profile, where asterisks denote location of pressure sensors and current meters.

THIS PAGE INTENTIONALLY LEFT BLANK

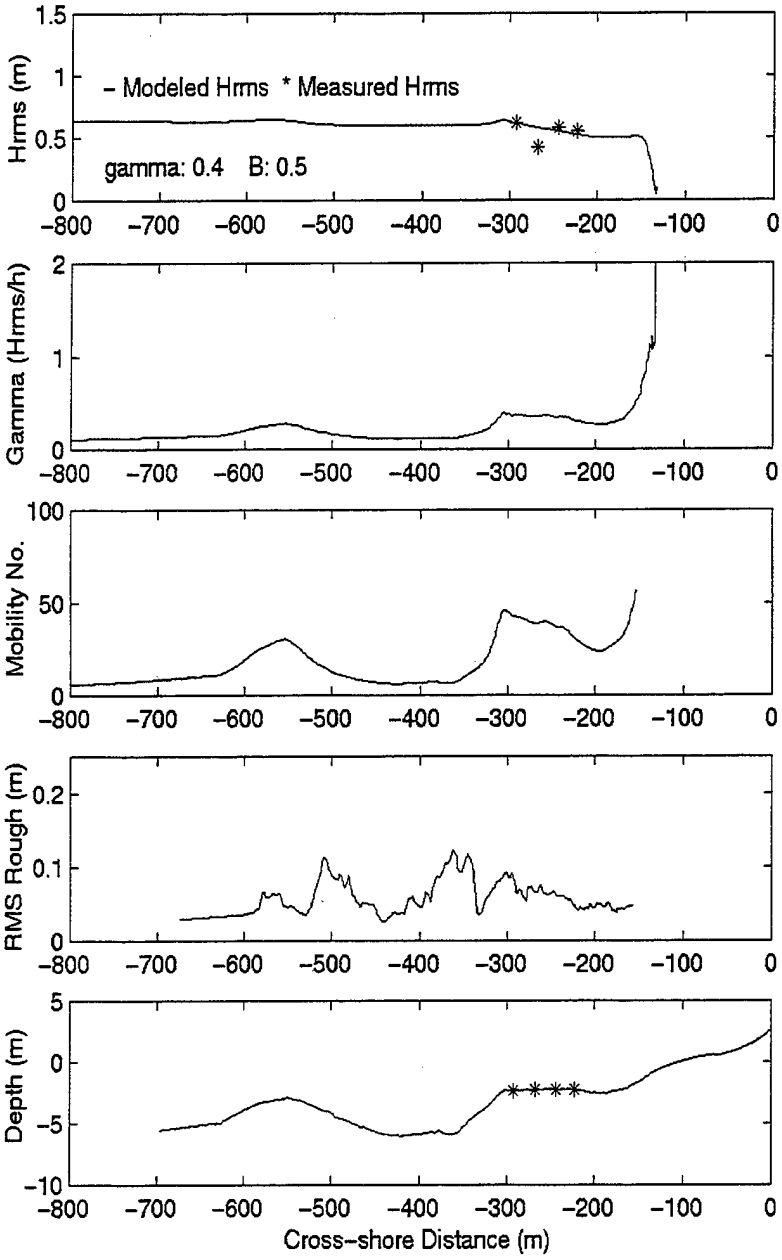

Figure 18. Cross-shore profiles for 8 Nov (at y=775 m on Fig. 13). a) modeled wave height, asterisks denote pressure meter measured wave heights. b) modeled gamma; c) mobility number calculated from modeled wave heights, d) roughness profile; and e) cross-shore depth profile, where asterisks denote location of pressure sensors and current meters.

THIS PAGE INTENTIONALLY LEFT BLANK

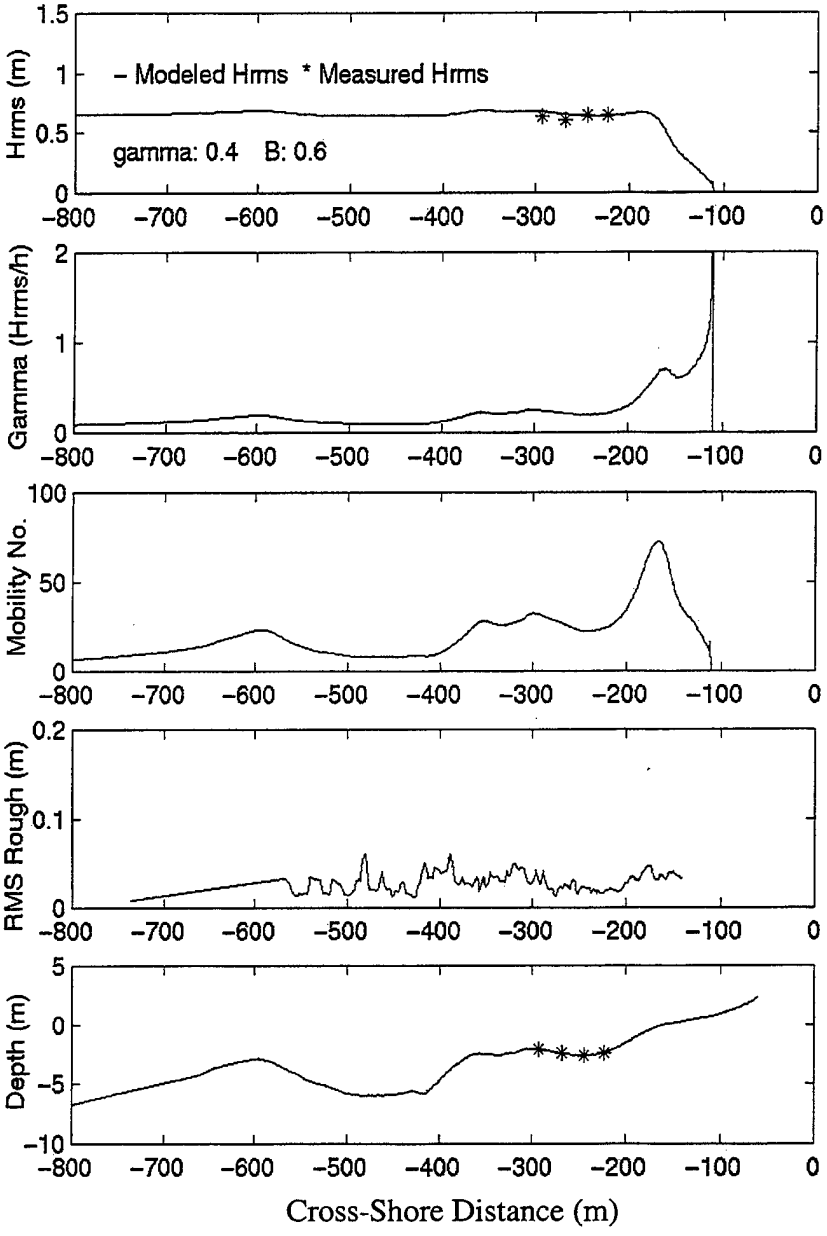

Figure 19. Cross-shore profiles for 15 Nov (at y=775 m on Fig. 14). a) modeled wave height, asterisks denote pressure meter measured wave heights. b) modeled gamma; c) mobility number calculated from modeled wave heights, d) roughness profile; and e) cross-shore depth profile, where asterisks denote location of pressure sensors and current meters.

THIS PAGE INTENTIONALLY LEFT BLANK

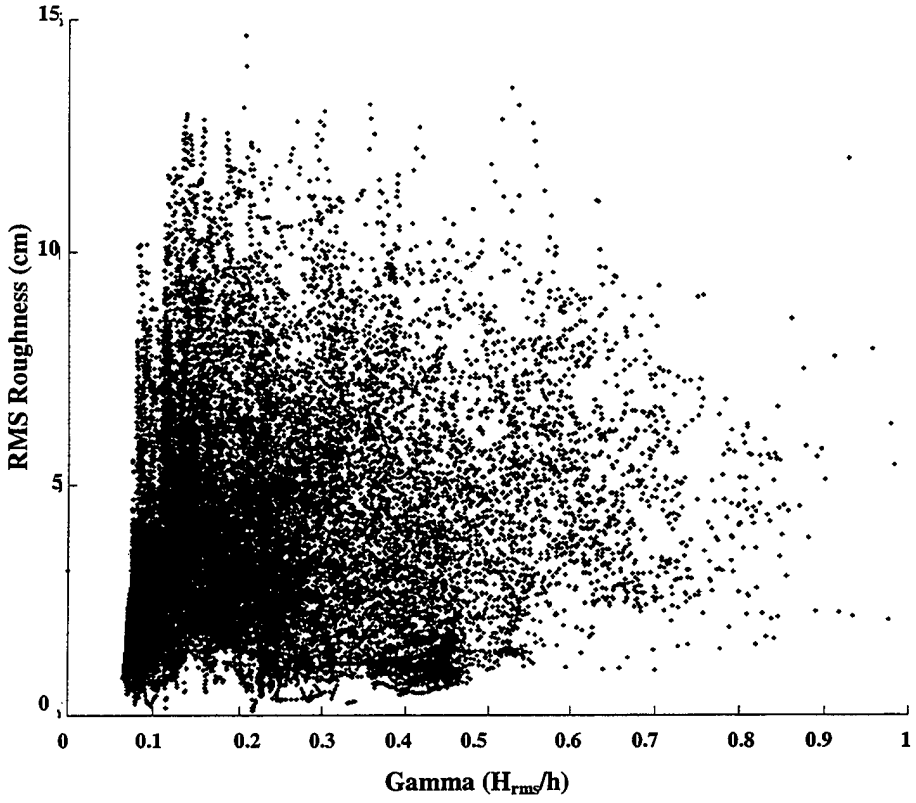

Figure 20. Roughness versus gamma for the whole COAST 3D Experiment.

THIS PAGE INTENTIONALLY LEFT BLANK

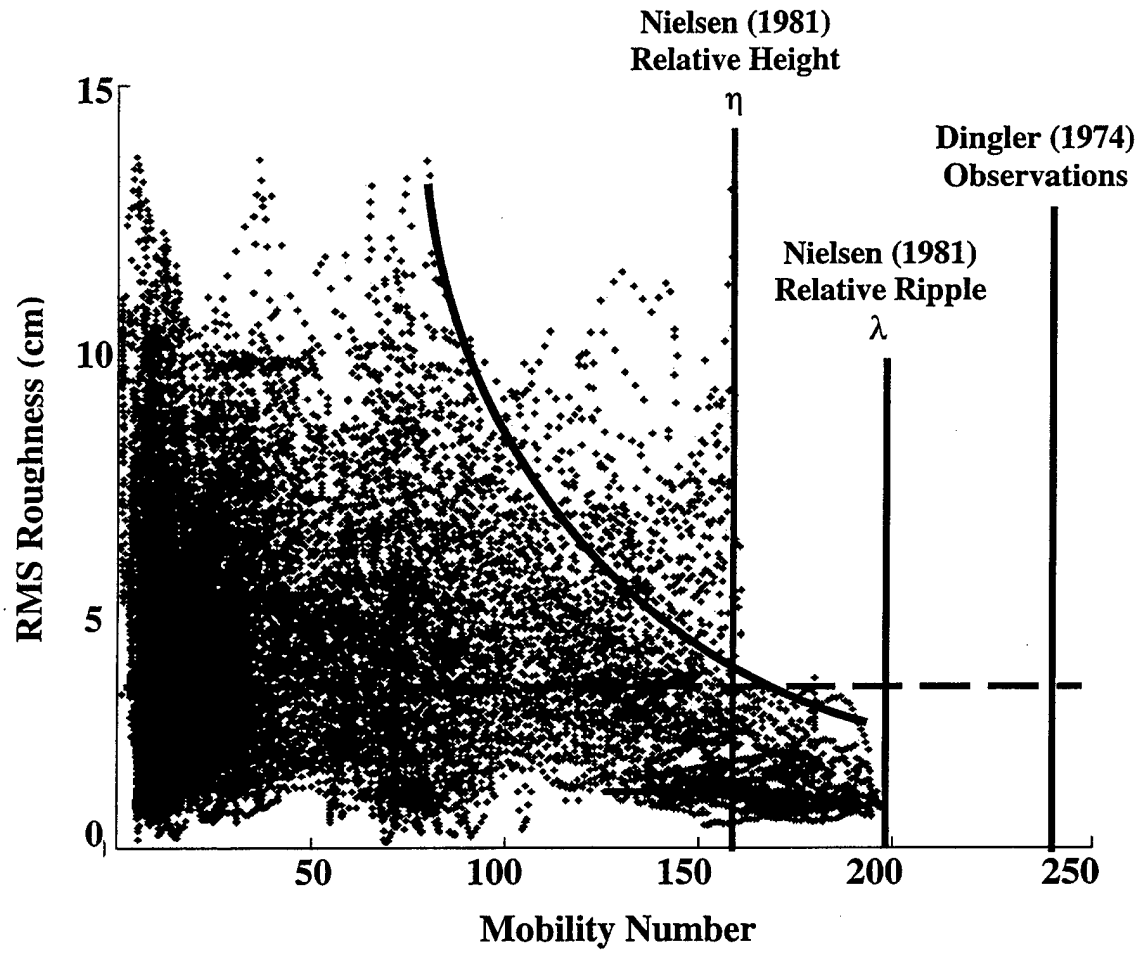

Figure 21. RMS roughness versus mobility number derived from predicted wave heights. The plane bed thresholds of Dingler (1974), and Nielsen (1981) using relative ripple height and relative ripple wave length are shown. The curve illustrates gradual decrease in roughness as mobility number increases to plane bed threshold. Dashed line is the lower limit at which the sonar altimeters can resolve ripples during this study.

THIS PAGE INTENTIONALLY LEFT BLANK

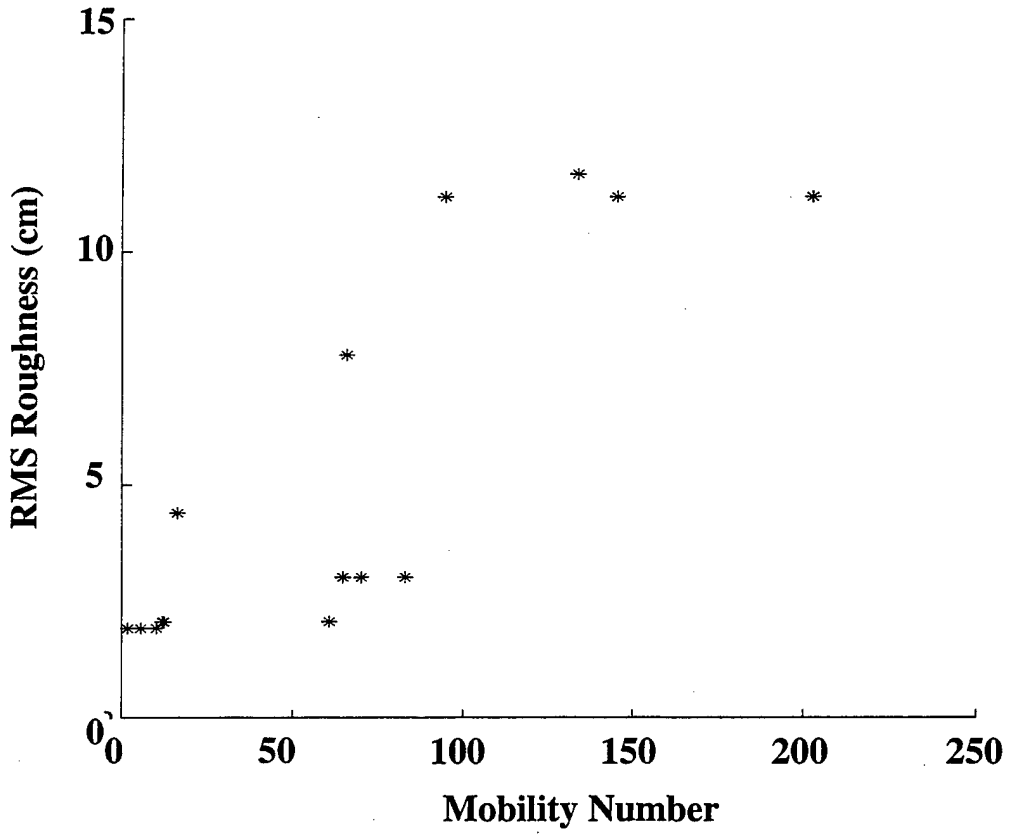

Figure 22. RMS Roughness versus mobility number derived from current meter measurements.

THIS PAGE INTENTIONALLY LEFT BLANK

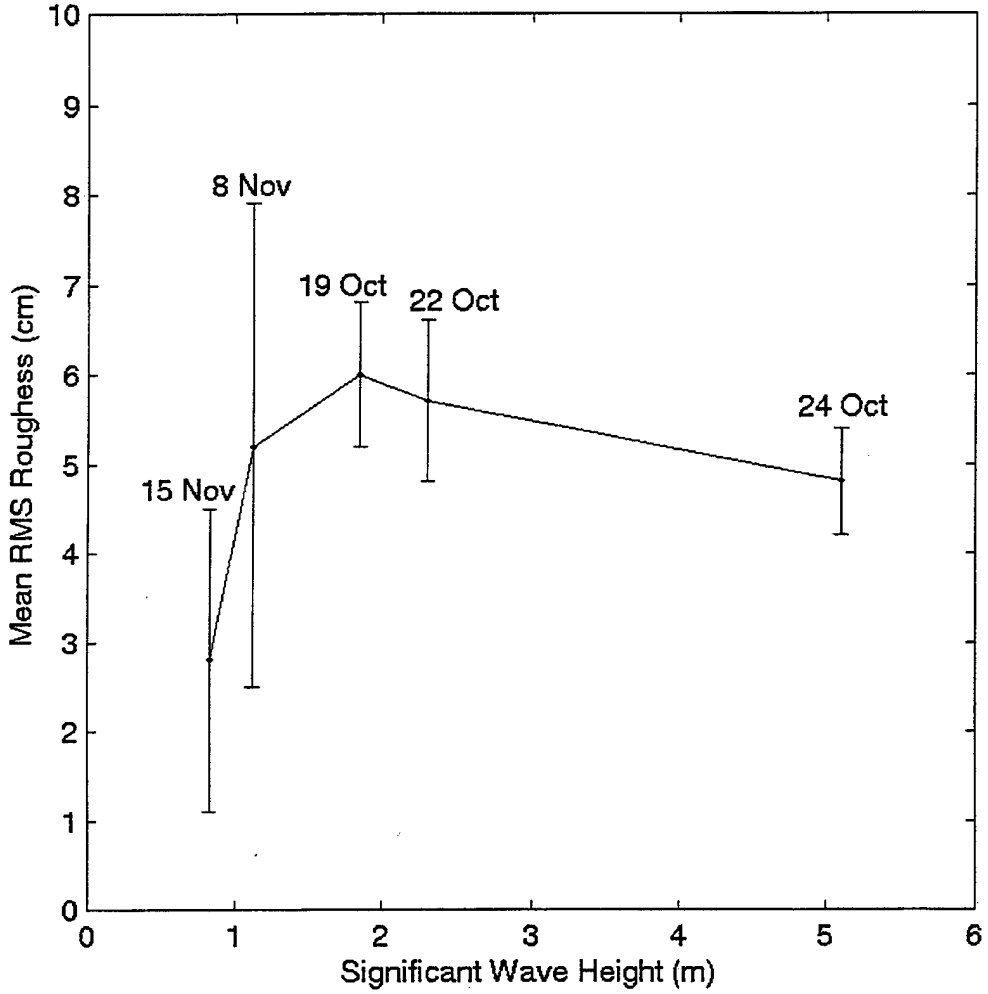

Figure 23. Mean (over a whole survey) RMS roughness versus significant wave height. Bars represent standard deviation of RMS roughness.

THIS PAGE INTENTIONALLY LEFT BLANK

LIST OF REFERENCES

Clifton, H.E., Hunter, R.E. and R.L. Phillips, Depositional structures and processes in the non-barred high-energy nearshore, *Journal of Sedimentary Petrology,* 41 (3), 651-670, 1971.

Clifton, H.E., Wave-formed Sedimentary Structures-A Conceptual Model, *Beach and Nearhshore Sedimentation,* edited by R.A. Davis, Jr. and R.L. Ethington, SEPM Special Pub. 24, 126-148, 1976.

Davidson-Arnott, R.G.D., and Greenwood, B., Facies relationships on a barred coast, Kouchibouguarc Bay, New Brunswick, Canada, In Davis and Ethingtion ed: *Beach and Nearshore Sedimentation, SEPM Special Publication, 24,* 149-168, 1976.

Dingler, J.R. and Clifton, H.E., Tidal cycle changes in oscillation ripples on the inner part of an estuarine sand flat, *Marine Geology*, 60, 219-233, 1984.

Dingler, J.R. and Inman, D.L., Wave Formed Ripples in Seashore Sands, In: *Proceedings 15th Coastal Engineering Conference, ASCE,* 2109-2126, 1976.

Dingler, J.R., Wave formed ripples in nearshore sands, Ph. D. thesis, University of California, San Diego, 136pp, 1974.

Fredsoe, J. and Diegaard R., Mechanics of Coastal Sediment Transport, Advanced Series on Ocean Engineering, 3, *World Scientific*, 369pp, 1992.

Gallagher, E.L., Boyd, W., Elgar, S., Guza, R.T., and Woodward, B., Performance of a sonar altimeter in the nearshore, *Marine Geology,* 133, 241-248, 1996.

Gallagher, E.L., Elgar, S., and Guza, R. T., Observations of sand bar evolution on a natural beach, *Journal of Geophysical Research*, 103, 3203-3215, 1998.

Gallagher, E.L., Thornton, E.B., and Stanton, T.P., Sand bed roughness in the nearshore, (awaiting submission), 2000.

Greenwood, B., Richards, R.G., and Brander, R., Acoustic imaging of seabed geometry: a high resolution remote tracking sonar (HRRTS II), *Marine Geology*, 112, 207-218, 1993.

Hay, A.E. and D.J. Wilson, Rotary sidescan images of nearshore bedform evolution during a storm, *Marine Geology,* 119, 57-65, 1994.

Hay, A.E. and Wilson, D.J., Spatially corrected depth changes in the nearshore zone during autumn storms, *Journal of Geophysical Research*, 98, 12387-12404, 1993.

Inman, D.L., Wave generated ripples in nearshore sands, *Beach Erosion Board, U.S. Army Corps of Engineers, Tech Memo*, 100, 1957.

Komar, P.D. and Miller, M.C., The threshold of sediment movement under oscillatory water waves, *Journal of Sedimentary Petrology*, 43, 1101-1110, 1973.

Krone, A., Hoekstra, P., Houwman, K., and Ruessink, G., COAST 3D: Description of the Egmond Fieldsite, *COAST 3D Kick-off Workshop Report*, 3, 36pp, 1997.

Middleton, G.V. and Southard, J.B., Mechanics of Sediment Movement, *Lecture for short course no. 3, Society of Economic Paleontologists and Mineralogists,* 7.1-7.68, 1982.

Miller, M.C. and Komar, P.D., A field investigation between oscillation ripple spacing and the near-bottom water orbital motions, *Journal of Sedimentary Petrology*, 50, 180-191, 1980.

Mulder, J., Coastal Zone Management (CZM) Tools and Guidelines; View of an End User, *COAST 3D Kick-off Workshop Report*, 2, 2pp, 1997.

Nielsen, P., Coastal Bottom Boundary Layers and Sediment Transport, *World Scientific Publishing Co.*, 102-145, 1992.

Nielsen, P., Dynamics and geometry of wave-generated ripples, *Journal of Geophysical Research,* 86, 6467-6472, 1981.

Ruessink, B.G., Van Enckevot, I.M.J., Kingston, K.S., and Davidson, M.A., Observations of two- and three-dimensional sandbar behaviour, *Marine Geology* (awaiting acceptance), 2000.

Southard, J.B. and Boguchwal, L.A., Flume experiments on the transition from ripples to lower flat bed with increasing grain size, Journal of Sedimentary Petrology, 43, 1114-1121, 1973.

Thornton, E.B., J.L. Swayne, and R.M. Dingler, Small-scale morphology related to waves and currents across the surf zone, *Marine Geology,* 145, 173-196, 1997.

Thornton, E.B. and Guza, R.T., Transformation of wave height distribution, *Journal of Geophysical Research*, 88(C10), 5925-5938, 1983.

Vincent, C.E. and Osborne, P.D., Bedform dimensions and migration rates under shoaling and breaking wave, *Continental Shelf Reseach*, 13, 1267-1280, 1993.

Wright, L.D., Boon, J.D., Green, M.O., and List, J.H., Morphodynamics of a bar-trough surf zone, *Marine Geology*, 70, 251-285, 1986.

INITIAL DISTRIBUTION LIST

No. of Copies

1. Defense Technical Information Center 2
   8725 John J. Kingman Rd., STE 0944
   Ft. Belvoir, Virginia 22060-6218

2. Dudley Knox Library. 2
   Naval Postgraduate School
   411 Dyer Rd.
   Monterey, California 93943-5101

3. Oceanography Department, Code OC/Gd. 1
   Naval Postgraduate School
   833 Dyer Rd., Rm. 328
   Monterey, California 93943-5122

4. Prof. E.L. Gallagher. 2
   Oceanography Department, Code OC/Ga
   Naval Postgraduate School
   833 Dyer Rd., Rm. 328
   Monterey, California 93943-5122

5. Prof E.B. Thornton. 2
   Oceanography Department, Code OC/Tm
   Naval Postgraduate School
   833 Dyer Rd., Rm. 328
   Monterey, California 93943-5122

6. LCDR Robert L. Kendall. 4
   OA Division
   USS JOHN C STENNIS
   FPO AP 96615-2874

7. Commander 1
   Naval Meteorology and Oceanography Command
   Stennis Space Center, MS 39529-5000

8. Mr. James J. Kendall 1
   2024 50th St., N.W.
   Canton, Ohio 44709

THIS PAGE INTENTIONALLY LEFT BLANK